A Humanoid Robot Pushing Model Inspired by Human Motion

A Thesis

Submitted to the Faculty

of

Drexel University

by

Alexander N. Alspach

in partial fulfillment of the

requirements for the degree

of

Master of Science in Mechanical Engineering and Mechanics

June 2012

Dedication

This thesis is dedicated to my family and friends all over the world.
No matter where I am, I know that it's where I should be.

Acknowledgments

For giving me the ability to live and learn among those of a like mind, I thank every member of Drexel's Autonomous Systems Lab (DASL). Without you, the successes I have realized over the last five years would not have been possible.

For adopting me as one of your own and making me comfortable so far from home, a warm thanks to Dr. Jun Ho Oh and my brothers at the HUBO Lab in Daejeon, South Korea.

For cultivating my passion in robotics and supporting my ventures to places I would otherwise never have gone, Dr. Paul Oh, I appreciate all that you have done for me.

For the burning of countless barrels of midnight oil, a special thanks goes to my labmate, Youngbum Jun, for tirelessly working with me to finish this research.

And for supporting my endeavor into engineering and robotics from an early age, my deepest gratitude is owed to my parents, Margaret and Henry, and my brother, Reed. My middle school toying with a LEGO Mindstorms kit is the inspiration of my engineering degrees and an exciting career to follow.

Table of Contents

List of Figures

Abstract

A Humanoid Robot Pushing Model Inspired by Human Motion
Alexander N. Alspach
Paul Y. Oh, Ph.D.

This thesis explores an observed method used by humans when pushing a large object of unknown mass. Body motion and reaction forces are analyzed for feet-apart pushing with varying stance length. It is found that, via articulation of the waist, a human will push their static zero-moment point (ZMP) as far forward as possible prior to pushing. Along with an extended back leg, this provides a larger support region in which the ZMP can move before stability is lost. Using this motion, the subject can produce a larger force than if the waist is constrained. Further, in this stance the subject is stable without object contact and can exert a range of forces by controlling mass distribution at the feet. For this increases in force exertion and stability, a linearized double inverted pendulum model with a feet-apart stance is proposed for use in the humanoid robot pushing of an unknown mass. Using the human pushing data and our humanoid, HUBO+, the advantage of this model and the added degree of freedom is shown against the commonly used single inverted pendulum model for humanoid robot pushing.

Chapter 1: Introduction

This thesis will present the work done in pursuit of a mathematical model suited to the form of a humanoid robot for the pushing of an unknown mass. In Chapter 2, the motivation for such research will be established, and in Chapter 3, current methods of humanoid pushing will be evaluated. The concept of the zero-moment point (ZMP) stability criterion, as well as a formulation of single and double inverted pendulum humanoid models will be presented in Chapter 4.

In Chapter 5, the motion and reaction forces of the human body while pushing a fixed object will analyzed to determine the applicability of the double inverted pendulum model. These observations are used to design the humanoid pushing experiment found in Chapter 6. Finally, the results of said experiment will be discussed in Chapter 7. Through this research, it was found that a larger range of forces can be exerted when taking advantage of the stability of a feet-apart stance and the added degree of freedom allowed by the double inverted pendulum model over a single inverted pendulum model for a humanoid robot.

Chapter 2: Motivation

Using our ability to critically consider the problems we face and logically arrive at a solution, we humans have developed and utilized countless tools and techniques to make our lives easier, safer and more efficient. These tools and the way in which they are used have advanced alongside the human mind over the past two hundred-thousand years. Now we can start fires with the flick of a finger, we can travel halfway around the world in a day and we can produce the planes that take us there in an automated factory using robotic arms that move heavy loads, weld, and assemble products with a dexterity and precision unmatched by man. As the desire for more comfortable, fruitful lives evolves, so does the demand for tools that can help us do more with less input. Autonomous machines, or robots, are designed to satisfy this ever growing desire.

While fascination and investment in robotic systems is growing worldwide, most robots lack the versatility to perform more than one specific task. While the future of robotics often explored in science-fiction depicts a family friendly and abundantly functional companion, today's robots are found in our militaries, factories and exploration endeavors. Robots have helped us efficiently mass produce some of our most complex developments like vehicles and computers. Robots have also explored the frontiers, both terrestrial and extraterrestrial, that humans have neither touched nor seen firsthand. Robots help us locate and rescue people in disaster situations and

help us fight wars with less lives lost. Now robots can even be found in some homes cleaning floors or pools while the owner is out for the day. While some applications of these automated systems are more significant than others, the fact remains that a robot can be designed to do an otherwise human job effectively and consistently in any given environment, including those places where a human dare not go. The shortcoming of these systems is adaptability. For a solution, we look to ourselves for inspiration.

Humanoid robots, designed to mimic humans in both form and function, come with the philosophy that a robot designed to do *our* jobs in *our* environments should share *our* likeness. With two legs, a humanoid robot has the ability run and jump, step over obstacles, climb stairs, use ladders and even control our vehicles. With two arms and two free hands, the robot can use our tools and appliances and manipulate the world around it. A humanoid robot could more accurately and effectively replace a human doing tedious or dangerous work than a robot of any other form by using human tools to complete human tasks. Further, a humanoid robot can be designed to be more powerful and more capable than a human when manipulating massive objects or working tirelessly without rest. Researchers of humanoid robotics are striving towards a near future of multipurpose robots that can intelligently carry out a high-level directive in unstructured and likely unknown environments. Think *employees*, not *tools*.

Humanoid research usually pertains to either the lower body or the upper body. While some researchers focus on bipedal mobility and stability on varying terrains, others are focusing on environmental perception and manipulation. Full body motion

is a relatively new field of research and considers the static and dynamic stability of the robot as it accelerates and positions its upper body, arms and anything it may be carrying. Full body stability must also be considered when the robot is enduring some external force or applying a force to its environment. Currently, the humanoid's ability to impact its environment remains underdeveloped. While humanoids commonly demonstrate dexterous manipulation of small, known objects, interaction with heavier objects and impulsive forces may cause disturbances too large for standard stability techniques to compensate. To achieve the goal of aiding and replacing humans in our working environments, human-like environmental interactions using full-body motion and force generation must be further explored and developed.

When imparting a large force to the environment, a human will utilize his entire body to develop a mechanical advantage. For pushing, pulling or wielding a heavy object or tool, a stable stance is found with all points of contact considered. Stability is found when the Zero-Moment Point (ZMP), or the point on the ground where the summation of all reaction moments equals zero, falls within the support polygon, or the convex hull area created by the body's points of contact. This concept of ZMP is defined in Chapter 4. When producing a pushing force, a human's stance often consists of either one foot or both feet displaced some distance from the object being pushed. Hereafter, these two common stances will be called the feet-apart pose and the feet-together pose, respectively, and are illustrated in Figure 2.1.

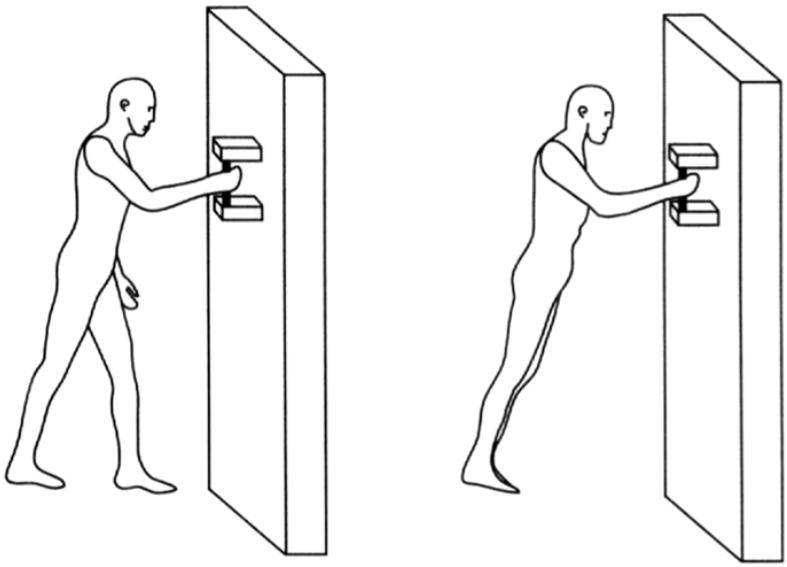

Figure 2.1: Human pushing on a fixed handle in a feet-apart posture (**left**) and a feet-together posture (**right**). Adapted from Rancourt and Hogan,"Dynamics of Pushing", 2001. [1]

An angled-body posture, by displacing the center of mass (CoM) both forward and downward, can help reduce the amount of torque that the pushing ankle needs to counteract. The statically displaced CoM also causes a component of the pusher's weight to factor into the horizontal pushing force exerted. In the case of a sudden decrease in force at the hands (e.g. static friction is overcome and the object moves), leaving one foot up front, as in the feet-apart pose, provides instant stability. This front foot placement allows for the ZMP to move forward some amount without loss of stability. This means that a person can also lean forward and continue pushing a moving object until they can no longer reach. Further, freedom to bend and translate the waist allows the upper body CoM, and therefore the ZMP, to be placed further forward prior to pushing, creating an even larger margin for ZMP movement when pushing. The necessity of at least one foot displaced from the pushing plane can

be illustrated by a human pushing a heavy object in a straight-up posture with parallel foot placement. The force at the hands causes a moment about the ankles and moves the ZMP posteriorly. The ZMP's leaving of the relatively small support polygon coincides with the tipping backward of the pusher. In the feet-apart pose, this ZMP can be displaced much further before exiting the support polygon and causing instability.

The feet-apart stance has been tuned by the human form, allowing a large stability margin and the exploration of a range of forces without moving the feet. It is worth exploring in detail how our methods of stably positioning and subsequently exerting force are executed so that a humanoid robot may do the same. Such research will allow humanoids to help or replace people in moving heavy objects, pushing loaded carts, applying force when using certain tools, or clearing heavy debris.

In this paper, the human method of pushing a static object is analyzed. Using a motion capture system and force-sensing plates, the movements of the body for varying displacements of the rear foot, along with the associated reaction forces produced at the hands and feet, are analyzed. Knowledge gained from this analysis on the ability to modulate force and maintain a stable pushing stance via upper and lower body orientation supports the use of a linearized double inverted pendulum model (DIVP), along with a feet-apart pose, when designing the pushing algorithms of a humanoid robot for an object of unknown mass.

Chapter 3: Literature Review

Although the field of humanoid robot-based research is still in its infancy, the groundwork for humanoid design and stable biped locomotion was being laid in the early 1970s. The first full-sized anthropomorphic robot in the world, WABOT-1, was developed at Waseda University in Tokyo, Japan. This robot was a research platform for computer vision, Japanese language recognition and synthesis, tactile sensing, manipulation and basic static walking. This research lead to the development of WABOT-2 in the early 1980s. Both robots were used primarily as platforms for research in artificial intelligence and human-robot interaction [3].

Honda began work on their first iteration of what is now known worldwide as ASIMO in 1986 and released a humanoid robot to the public 11 years later [4]. From 1986 to 1993, Honda developed its E-series robots (Experimental Models 0-6) which had two legs and a large body but no arms. The E2 was the first biped robot to demonstrate human-like dynamic walking. Using this robot, Honda also developed algorithms for autonomously balanced stair climbing, sloped plane walking and stepping over obstacles. From 1993 to 1997, the P-series (Prototype Models 1-3) were in development. These were the anthropomorphic predecessors of ASIMO. Now with arms and hands, research could be done on object transportation and manipulation. This robot was designed to mimic a human's mass distribution as much as possible while maintaining most of the same proportions. The new arms

contained force-torque sensors for force control and had six degrees of freedom (DOF) each [5]. Released in 2000, ASIMO (54kg, 1.3m, 34DOF) exhibited the culmination of all that Honda learned from their prior humanoids [6]. ASIMO was designed to work alongside humans and exhibited Honda's research into more artificially intelligent and autonomous systems. Using a binocular vision system, the robot could navigate to a location while avoiding obstacles. The robot could also recognize faces that it had seen before and human hand gestures like handshakes, waves, beckons and pointing at an object. ASIMO can also walk on uneven terrain, run, jump, climb stairs and avoid moving obstacles while walking [7]. The most recent iteration of ASIMO was demonstrated by Honda in 2011 [8].

During this private and largely unpublished exploration by Honda, academic research universities continued development in humanoid robotics. Waseda University developed another robot, WABIAN (107kg, 1.66m, 35DOF), in 1995 [9]. Using WABIAN, Yamaguchi et al. developed control algorithms for compensating dynamic motion of the arms while walking. This full-body dynamic stability was achieved by modeling the entire robot as a system of particles and compensating for shifts in the dynamic ZMP using three-axis trunk motion. In 1998, Japan's National Institute of Advanced Industrial Science and Technology (AIST), along with Kawada Industries, Inc., produced their first humanoid robotic platform, the HRP (130kg, 1.6m, 28DOF) [10], and, after five more versions, came out with HRP-4 (39kg, 1.51m, 34DOF) in 2011 [11]. The HRP-4 was developed for adoption as a main humanoid research platform for companies and academic institutions. This full-sized humanoid, developed for the consumer, was designed to be lightweight and low cost, using common parts

and joint designs throughout the robot. International safety standards were considered and motor power output and force output were limited to comply. In 2001, the Technical University of Munich presented the development of their robot, Johnnie (37kg, 1.8m, 17DOF), designed to realize dynamically stable walking and jogging motions [12]. Beginning humanoid research in 2000, Korea's Advanced Institute of Science and Technology (KAIST) unveiled HUBO (55kg, 1.25m, 41DOF) in 2005 [13]. KAIST's Dr. Jun Ho Oh et al. presented the latest version of this robot, HUBO+ (45kg, 1.3m, 38DOF) in 2011. This robot, like the HRP-4, has been commercialized and has been adopted as the shared research platform for collaboration between KAIST, Drexel University and a handful of other United States universities.

With many years of mechanical design and iteration under the belts of those designing, many universities and research institutions can forgo the development of their own humanoid platform and focus their research on other matters. The maturity and availability of these systems has spurred more rapid development in the areas of cognition, manipulation, locomotion, human-robot interaction and robot-environment interaction. The pushing and carrying of objects, otherwise known as whole body manipulation, must be explored if humanoids are to replace and aid human workers in the future.

3.1 Humanoid Robot Pushing

The use of the Zero-Moment Point (ZMP) [2] for humanoid robot stability was first proposed by Miomir Vukobratovic in 1968. In a static sense, and with no environmental contact except at the floor, The ZMP is equivalent to the system's center

of pressure (CoP) on the ground plane [14]. Keeping this point within the robot's support polygon ensures static stability. For example, in a static, single-support (one-legged) pose, the robot is most stable if the ZMP is at the center of the area of ground beneath the foot. In a double-support pose, the ZMP should be within either foot area or the area between the feet. If this point leaves the support polygon, it indicates the presence of an uncompensated moment on the foot. The robot will rotate about the point on the support polygon perimeter through which the ZMP exited and will likely fall over. This method implies that, in a static situation, the robots center of mass (CoM) should always be placed directly above this support polygon. This method can be extended from static to dynamic control applications by using a simplified mathematical model of the humanoid to predict the effect on ZMP location of the robot's body links as they accelerate in three dimensions. Commonly, this extension includes a wheeled-cart and inverted-pendulum model [15]. The consideration of dynamic forces allows control of stable dynamic walking [16], running [17, 18] and jumping [19] through monitoring and control of the ZMP location.

While the ZMP has mainly been used as a stability criterion where contact is only made with the ground, Harada et al. extended the definition to include the effects of external forces and moments at the robot's manipulators and the angular velocity about the center of mass [20]. In their paper on humanoid pushing manipulation, the generalized ZMP (GZMP) represents the ZMP if no external contact is made. The real ZMP includes the moment produced by the pushing reaction forces on the robot's hands. While the distance between the ZMP and GZMP locations is varied to control pushing force at the hands, the location of the GZMP can be controlled to ensure

stability while pushing. This pushing examination only considers the feet-together stance where both feet are in line and displaced back away from the object being pushed. When positioning to exert more force, the entire body must be repositioned to displace the robots feet further from the pushing plane. Without the support of the object, the robot is unstable. This research also assumes that the pushing force is known and that the manipulated object is relatively light.

Harada et al. extended their theories and provided an analytic walking gait for pushing objects of an unknown but relatively light mass [21]. This online gait generation consisted of two phases: one for pushing and the next for stepping. Impedance control was implemented to control the walking speed based on the reaction forces experienced at the hands. Again, for pushing, they used a feet-together pose with both feet displaced backward and an angled body. The problem of compensating for discontinuities in ZMP from changes of velocity between steps was never solved.

To overcome the limitations of Harada's work, Motoi et al. proposed a method of online gait generation for unknown mass object pushing, switching between double and single support phase (DSP and SSP, respectively) ZMP control while stepping [22]. In this method, the reference ZMP, or the ZMP plus the influence on ZMP from the force felt at the hands, is obtained in the DSP and used when pushing in the SSP. To avoid discontinuities in ZMP reference between iterations, the cycle time of the DSP is modified at each iteration.

Stilman et al. devised gait planning methods that allowed a humanoid robot to push a wheeled, weighted cart (with a mass of up to 55kg) along a two dimensional path to a goal position [23, 24]. The dynamic frictional model of the cart is learned

via experimental data so that the force necessary to perform certain maneuvers can be predicted over the specified path. This model is used to plan the stable humanoid motions offline. With this method, the path and gait cannot be modified online so the stability is subject to the accuracy of the model. Also, the robot's motions must be planned for a specific cart of a known mass and known dynamic behavior.

As opposed to the constant pushing force sought in the previously mentioned papers, Hwang et al. mathematically analyzed the the relationship between the shifting of ZMP and impulsive force generation for pushing a wall and turning a valve [25]. While this research explores the humanoid pushing of heavier objects, the results were demonstrated in simulation only and dynamic stability was ignored.

The object pushing methods discussed (Harada, Motoi, Stilman, and Hwang) have all utilized Kajita et al.'s three-dimensional linearized inverted pendulum model (3D-LIPM) to approximate the humanoid robot's dynamic behavior [26]. This model regards the humanoid as having massless legs and all mass concentrated at the CoM. While this model has proven to effectively simplify the control of humanoid stability for research in dynamic walking on rugged terrain and the rejection of disturbance from applied external forces, the model neglects the ability to use distributed mass to the robots advantage. When pushing a heavy object, it may prove worth the extra computation and mathematical complexity to leverage the characteristics of a model more closely resembling the structure and fundamental degrees of freedom of a humanoid body. The benefits of a linearized double inverted pendulum, along with the feet-apart stance, warrant exploration.

3.2 Human Force Exertion

Over the past 100 years, multiple studies have been performed to quantify a humans ability to exert force and to determine the effects of the different influencing variables on this ability. These studies were mainly conducted to direct the safety standards of the working environment for manual laborers.

In 1958, Dempster statically analyzed the efforts of a subject pulling at many different angles, above and below the head, in the sagittal plane [27]. Photographed at the point of maximum exertion, the subject-chosen configuration was distilled into a free body diagram and, using the pulling force vector and the effect of gravity, the reaction force at the feet was determined. This study located maximum bending moments throughout the body in an effort to find the joints limiting the maximum pulling force. It was found that the subject chose joint configurations when pulling that allowed his body weight to play a larger role in the exerted force those that of the muscles in the trunk and limbs. The configurations involved moving the center of mass as far from center of pressure at the feet as possible, creating a moment about the ground contacting point and a corresponding force at the hands.

Chaffin, Andres and Garg confirmed these results in 1983 and explored the effects of handle height and foot placement variations on force exerted [28]. In this study, subjects were given pushing and pulling tasks in which they could pick any joint configuration they saw fit for exerting the largest forces possible.

Ayoub and McDaniel published the effects of stance on pushing and pulling tasks using a sample of 46 people in 1974. The postural data was analyzed to provide the

general hand and foot positions necessary for the efficient and safe exertion of force. For pushing, it was found that the best location for the exertion of force at the hands (i.e. the location of a handle) is at 70% of the subject's shoulder height with a rear foot placed posteriorly at 100% of the subject's shoulder distance from the plane of pushing [29].

In 1993, Daams brought into question these methods of testing human pushing. It was proposed that, while standardized postures are easiest to analyze, they may not accurately represent the methods used in the real-life situations where force exertion is necessary [30]. It was determined that testing subjects given more degrees of freedom produces more reliable and reproducible results.

Rancourt and Hogan (2001), rather than studying just the maximum force exerted in a given stance, studied the ability to modulate force at the hands [1]. The effects of body angle, hand torque, vertical hand force and the lifting of a leg to raise ones center of mass were calculated and shown to allow for small variations in force exerted. The effect of a feet-together pose versus a feet-apart pose (Figure 2.1) was also explored. It was evaluated that, with just one foot displaced back and the other left up front, pushing forces were an order of magnitude higher than those exerted in an upright and statically stable pose. Further, while allowing the center of mass to be displaced more drastically while maintaining stability, the force at the hands could be varied between zero and some maximum force without changing the stance or the locations of the feet.

Chapter 4: Formulation

4.1 Zero-Moment Point (ZMP)

First proposed by Vukobratovic and Stepanenko in 1972, the zero-moment point (ZMP) criterion has become one of the most widely used stability criterion for legged robots.

For a single robot foot with no adhesion to the floor, the distributed foot-ground reaction forces can be reduced into a single resultant force acting at some point within the area of said foot (Figure 4.1). The point at which this localized resultant force acts is defined as the ZMP [2].

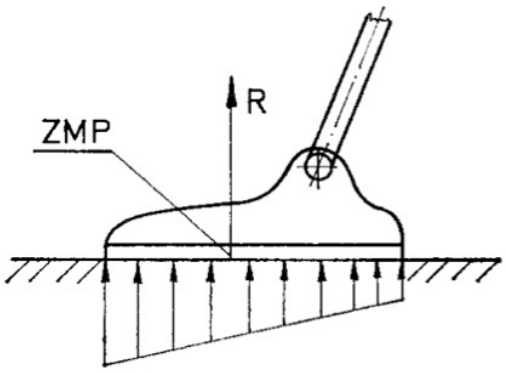

Figure 4.1: Distributed force resultant and coinciding zero-moment point (ZMP). Adapted from Vukobratovic and Stepanenko,"On the Stability of Anthropomorphic Systems", 1972. [2]

This concept can be extended for use on a robot with any number of ground-contacting points in three-dimensions. The ZMP definition and dynamic formulation presented in this paper will follow the definition and formulation presented by Shuuji

Kajita and Bernard Espiau in the Springer Handbook of Robotics (2008, pgs. 371-375) [31].

For a finite number of ground-contacting points $\mathbf{p}_i, (i = 1, 2, ..., N)$, the force vector acting at each point $\mathbf{p}_i$ can be defined as

$$\mathbf{f}_i = [f_{i,x} \ f_{i,y} \ f_{i,z}]^\top \ , \tag{4.1}$$

where the forces $f_{i,x}$, $f_{i,y}$ and $f_{i,z}$ are the components of f_i acting in the x, y and z directions of a ground-fixed coordinate system with an upward pointing positive z-axis. In this case, the ZMP can be defined as

$$\mathbf{p} = \frac{\sum_{i=1}^{N} \mathbf{p}_i f_{i,z}}{\sum_{i=1}^{N} f_{i,z}} \ . \tag{4.2}$$

The ZMP can also be represented as

$$\mathbf{p} = \sum_{i=1}^{N} \alpha_i \mathbf{p}_i \ , \tag{4.3}$$

$$\alpha_i = f_{i,z}/f_z \ , \tag{4.4}$$

$$f_z = \sum_{i=1}^{N} f_{i,z} \ . \tag{4.5}$$

Since all z-axis forces act in the same direction (i.e. no adhesion between the

contact surface and the ground),

$$\begin{cases} \alpha_i \geq 0, & \text{(i=1, 2, ..., N)} \\ \sum_{i=1}^{N} \alpha_i = 1 \ . \end{cases} \tag{4.6}$$

Due to the constraint of only upward acting reaction forces, all of the points on the ground plane that satisfy equations (4.3) and (4.6) are found within the convex hull outlined by the supporting surfaces, or the support polygon. For a stable robot, the ZMP is always within this support polygon.

The torque about the ZMP can be defined as

$$\boldsymbol{\tau} = \sum_{i=1}^{N} (\mathbf{p}_i - \mathbf{p}) \times \mathbf{f}_i \ . \tag{4.7}$$

In terms of its vector components, this torque about the ZMP can be redefined as

$$\boldsymbol{\tau}_x = \sum_{i=1}^{N} (p_{i,y} - p_y) f_{i,z} - \sum_{i=1}^{N} (p_{i,z} - p_z) f_{i,y}, \ , \tag{4.8}$$

$$\boldsymbol{\tau}_y = \sum_{i=1}^{N} (p_{i,z} - p_z) f_{i,x} - \sum_{i=1}^{N} (p_{i,x} - p_x) f_{i,z}, \ , \tag{4.9}$$

$$\boldsymbol{\tau}_z = \sum_{i=1}^{N} (p_{i,x} - p_x) f_{i,y} - \sum_{i=1}^{N} (p_{i,y} - p_y) f_{i,x}, \ , \tag{4.10}$$

where $p_{i,x}$, $p_{i,y}$ and $p_{i,z}$ are the components of position vector $\mathbf{p}_i$ and p_x, p_y and p_z are components of the ZMP position vector, $\mathbf{p}$. On a horizontal plane, $p_{i,z} = p_z$ so,

through substitution of equation (4.2) into (4.8) and (4.9), we see that

$$\boldsymbol{\tau}_x = \boldsymbol{\tau}_y = 0 \ , \tag{4.11}$$

hence the name *zero-moment point* for $\mathbf{p}$. friction between the feet and the ground cause the moment about the z-axis (4.10) to be nonzero.

$$\boldsymbol{\tau}_z \neq 0 \ . \tag{4.12}$$

4.1.1 3-D Dynamic ZMP

For a three-dimensional robot of N rigid-body links, the ZMP can be computed in the ground-fixed coordinate system. The robot's total mass M and its center of mass location CoM are

$$M = \sum_{j=1}^{N} m_j \ , \tag{4.13}$$

$$\mathbf{CoM} = \sum_{j=1}^{N} m_j \mathbf{c}_j / M \ , \tag{4.14}$$

where m_j and $\mathbf{c}_j$ are the mass and center of mass location of the j-th link, respectively.

For this system, the total linear momentum is

$$\mathcal{P} = \sum_{j=1}^{N} m_j \dot{\mathbf{c}}_j \ , \tag{4.15}$$

and the total angular momentum is

$$\mathcal{L} = \sum_{j=1}^{N} [\mathbf{c}_j \times (m_j \dot{\mathbf{c}}_j) + \mathbf{R}_j \mathbf{I}_j \mathbf{R}_j^\top \boldsymbol{\omega}_j] \ , \tag{4.16}$$

where $\mathbf{R}_j$, $\mathbf{I}_j$ and $\boldsymbol{\omega}_j$ are the 3×3 rotation matrix, inertia tensor and angular velocity of the j-th link, respectively, and $\mathbf{R}_j \mathbf{I}_j \mathbf{R}_j^\top$ is the inertial tensor with respect to the global frame fixed to the ground. From the laws of Newton and Euler, the change in linear and angular momenta lead to:

$$\mathbf{f} = \dot{\mathcal{L}} - M\mathbf{g} \ , \tag{4.17}$$

$$\boldsymbol{\tau} = \dot{\mathcal{L}} - \mathbf{CoM} \times M\mathbf{g} \ , \tag{4.18}$$

where $\mathbf{g} = [0 \ \ 0 \ -g]^\top$.

Now, if we exert some external force at the ZMP (located at $\mathbf{p}$), the torque at this point becomes

$$\boldsymbol{\tau} = \mathbf{p} \times \mathbf{f} + \boldsymbol{\tau}_{ZMP} \ , \tag{4.19}$$

where all components except the z-axis torque are zero. Substituting equations (4.17) and (4.18) into (4.19) gives

$$\boldsymbol{\tau}_{ZMP} = \dot{\mathcal{L}} - \mathbf{c} \times M\mathbf{g} + (\dot{\mathcal{P}} - M\mathbf{g}) \times \mathbf{p} \ , \tag{4.20}$$

which has the components

$$\boldsymbol{\tau}_{ZMP,x} = \dot{\mathcal{L}}_x - \mathbf{c} \times Mgy + \dot{\mathcal{P}}_y p_z - (\dot{\mathcal{P}}_z + Mg)p_y \ , \tag{4.21}$$

$$\boldsymbol{\tau}_{ZMP,y} = \dot{\mathcal{L}}_y - \mathbf{c} \times Mgx + \dot{\mathcal{P}}_x p_z - (\dot{\mathcal{P}}_z + Mg)p_x \ , \tag{4.22}$$

where

$$\boldsymbol{\tau}_{ZMP} = [\boldsymbol{\tau}_{ZMP,x} \ \boldsymbol{\tau}_{ZMP,y} \ \boldsymbol{\tau}_{ZMP,z}]^\top \ ,$$

$$\mathcal{P} = [\mathcal{P}_x \ \mathcal{P}_y \ \mathcal{P}_z]^\top \ ,$$

$$\mathcal{L} = [\mathcal{L}_x \ \mathcal{L}_y \ \mathcal{L}_z]^\top \ ,$$

$$\mathbf{CoM} = [x \ y \ z]^\top \ .$$

Because $\boldsymbol{\tau}_{ZMP,x} = \boldsymbol{\tau}_{ZMP,y} = 0$, we can calculate the ZMP using equations (4.21) and (4.22):

$$p_x = \frac{Mgx + p_z\dot{\mathcal{P}}_x - \dot{\mathcal{L}}_y}{Mg + \dot{\mathcal{P}}_z} \ , \tag{4.23}$$

$$p_y = \frac{Mgy + p_z\dot{\mathcal{P}}_y - \dot{\mathcal{L}}_x}{Mg + \dot{\mathcal{P}}_z} \ , \tag{4.24}$$

where p_z is the height of the floor.

Statically, the ZMP becomes the projection of the CoM onto the ground plane.

4.2 Robot Model

For the design of dynamically stable walking, running and pushing motion, a linearized inverted pendulum (IVP) model with a concentrated mass (Figure 4.2) is usually used estimate the location of the ZMP for the N-link humanoid robot.

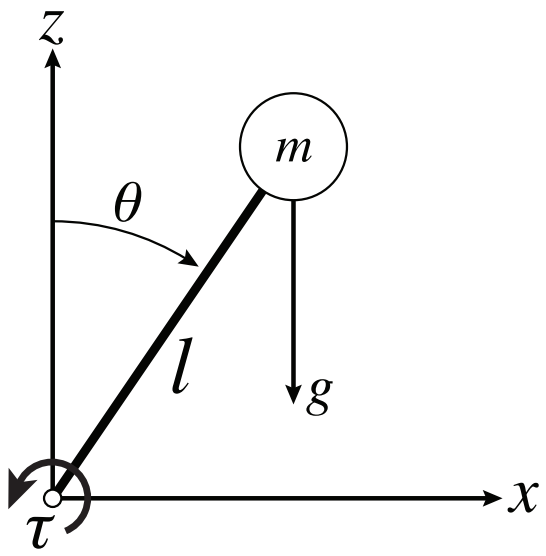

Figure 4.2: Inverted Pendulum (IVP) model

For this model, the dynamic equation of motion is

$$ml^2\ddot{\theta} + mgl\sin(\theta) = -\tau \ , \tag{4.25}$$

where m is the concentrated mass, l is the length of the link, θ is the angle from vertical to the link and τ is the torque at the joint.

For this single link, the ZMP, point p in equation (4.2), can be rewritten as

$$p = \frac{-\tau}{mg} \ . \tag{4.26}$$

where $\tau = pf$ and $f = mg$. Substituting equation (4.25) into (4.26), we obtain

$$p = \frac{ml^2\ddot{\theta} + mgl\sin(\theta)}{mg} \ . \tag{4.27}$$

Statically, equation (4.27) simplifies to

$$p = \frac{0 + mgl\sin(\theta)}{mg} = l\sin(\theta) \ . \tag{4.28}$$

This system, linearized using the small-angle approximation ($\sin(\theta) \approx \theta$) as per Kajita's method [26], can be simplified even further to

$$p = x \ , \tag{4.29}$$

where $l\sin(\theta) = l\theta$ and $l\theta = x$.

While the single inverted pendulum model is commonly used in humanoid robotics, it is much too simple of a model if the robot is to use the mass of its separate links to its advantage. Such is the case for the pushing of objects, as observed in human pushing and analyzed in Section 5.2. Having established the model for a linearized inverted pendulum, we can extend this formulation to that of the linearized *double* inverted pendulum model (Figure 4.3).

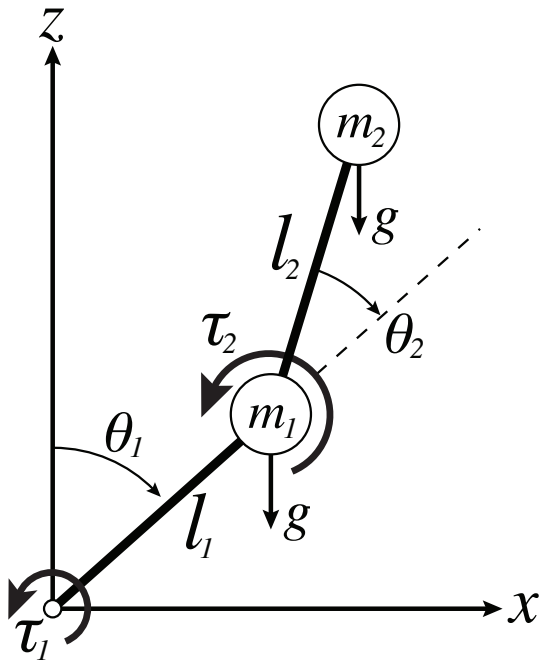

Figure 4.3: Double Inverted Pendulum (DIVP) model

For the double inverted pendulum, torque at the base of the lower link, link 1, is

$$\begin{aligned}\tau_1 &= \ddot{\theta}_1[l_1^2 m_2 + l_1^2 m_1 + l_2^2 m_2 + 2 l_1 l_2 m_2 \cos(\theta_2)] \\ &+ \ddot{\theta}_2[l_2^2 m_2 + l_1 l_2 m_2 \cos(\theta_2)] \\ &+ V(\theta, \dot{\theta}) + G(\theta) \ ,\end{aligned} \tag{4.30}$$

where

$$V(\theta, \dot{\theta}) = -l_1 l_2 m_2 \dot{\theta}_2^2 \sin(\theta_2) - s l_1 l_2 m_2 \dot{\theta}_1 \dot{\theta}_2 \ , \tag{4.31}$$

$$G(\theta) = -g l_1 m_2 \sin(\theta_1) - g l_1 m_1 \sin(\theta_1) - g l_2 m_2 sin(\theta_1 + \theta_2) \ . \tag{4.32}$$

$V(\theta, \dot{\theta})$ is the torque due to Coriolis acceleration and $G(\theta)$ is the torque due to gravitational acceleration.

The torque at the second joint is defined as

$$\begin{aligned}\tau_2 &= \ddot{\theta}_1[l_2^2 m_2 + l_1 l_2 m_2 \cos(\theta_2)] \\ &+ \ddot{\theta}_2(l_2^2 m_2) \\ &+ V(\theta, \dot{\theta}) + G(\theta) \ ,\end{aligned} \tag{4.33}$$

where

$$V(\theta, \dot{\theta}) = l_1 l_2 m_2 \dot{\theta}_1^2 \sin(\theta_2) \ , \tag{4.34}$$

$$G(\theta) = -g l_2 m_2 (\theta_1 + \theta_2) \ . \tag{4.35}$$

Again, we substitute the equation for torque at the base joint (4.30) into the equation for ZMP (4.26). Simplified for static use, the equation for the ZMP of a double inverted pendulum becomes

$$p = \frac{g l_1 m_2 \sin(\theta_1) + g l_1 m_1 \sin(\theta_1) + g l_2 m_2 sin(\theta_1 + \theta_2)}{(m_1 + m_2) g} \ . \tag{4.36}$$

This equation for ZMP will be used for the control and static analysis of the pushing stances assumed by the HUBO+ humanoid robot during testing.

Chapter 5: Human Pushing Analysis

The human form exhibits its adaptive characteristics in everything we do. To complete a task, a human can usually contort his numerous body links to fit in a defined space, traverse some undefined area, or exert a force on the environment utilizing some mechanical advantage. While these solutions may not be optimal, we find a way to complete the task. In pushing an object of unknown mass, an unknown force is required. In the initial consideration of this problem, it was noted that a human, presented with some large but unknown mass, will likely choose a feet-apart stance that consists of one leg extended and displaced back from the pushing plane with the other leg left up front for stability when positioning pre-push. The form of the feet-apart stance is illustrated in Figure 2.1 on page 5. Estimating the mass by size and experience only, the leg is displaced far back with the intention of exerting a larger force than necessary. An overestimation in this situation provides a longer support polygon and, therefore, a ZMP movement margin larger than necessary. The backward displacement of the ZMP location caused by the force at the hands will not exceed the limits of the support polygon unless the stance chosen was not long enough. In most cases, the overestimation will be enough and the person will increase the force at their hands until the object moves. Because, in this stance, a range of forces can be explored, the human is able to find the force necessary without constant reconfiguration. Comparing this pushing to the feet-together postures used in prior

humanoid pushing research, the study of the joint configurations and reaction forces experienced by humans in variations of feet-apart pushing became intriguing.

5.1 Experiment

The advantage of the previously described feet-apart pushing stance over a feet-together stance is the ability to lengthen one's support polygon for stability prior to the exertion of pushing force at the hands. To understand how this ZMP location is changed and contained within the support polygons of stances of differing lengths, the configuration of the body and the resulting forces exerted must be studied. Via motion capture data of the links composing the human body and force data at the body's points of contact with the ground and pushing surface, the shifts in ZMP location, the associated forces applied by the hands and the motions producing these results were recorded and analyzed for multiple test subjects.

5.1.1 Equipment

An OptiTrack 18-camera (V100:R2) motion capture system was used to capture the subject's body movements at 100 Hz. This system is focused on a 3x3 square meter section of the floor space with a visible height of 2.5 meters high. The subjects wore a motion capture suit fitted with 34 infrared-reflective markers. With four markers about the hips, three markers on the chest, head, each of the upper arms and hands, and two markers on each of the thighs, shins and feet, the subject's motions are tracked and mapped onto a three-dimensional skeleton of rigid-bodies. The rigid body locations, both global or relative to their parent link, along with the relative

Euler angles of each rigid body, can be exported as a delimited text file for analysis elsewhere.

The reaction forces at each foot and at the hands were recorded using custom force plates, a National Instruments (NI) USB-6211 data acquisition (DAQ) device, and a MATLAB graphical user interface (GUI) and data manager. A force plate was used at each of the subjects' contact points to record specific directional reaction forces at 100 Hz, allowing for ease of comparison with the motion capture data. These force plates were designed to each record force in one direction using one load-cell. The load-cell is sandwiched between a cantilevered aluminum square-beam and the wooden base of the force plate structure. The square beam is hinged 40 cm from the center of the load-cell contact point and is level when under no load. The pin about which the square beam rotates is captured by two large blocks that resist rotation and bending of the beam perpendicular to the free-rotation axis. The beam and pin were strong enough to resist torsion under the loads applied during testing. Spray tack was applied to the surface of the foot force plates to increase friction and eliminate slippage as a variable. A diagram of the force plates used for the reaction forces at the hands and at each foot can be seen in Figures 5.1 and 5.2, respectively.

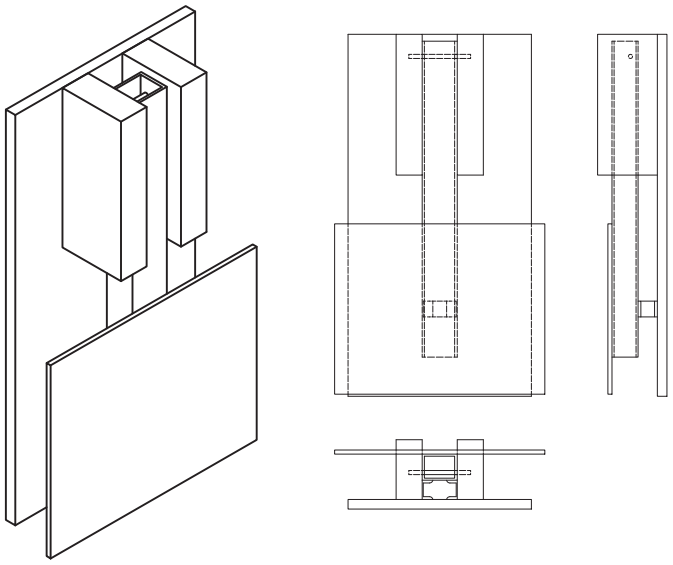

Figure 5.1: Diagram of force plates used to detect reaction force at the hands

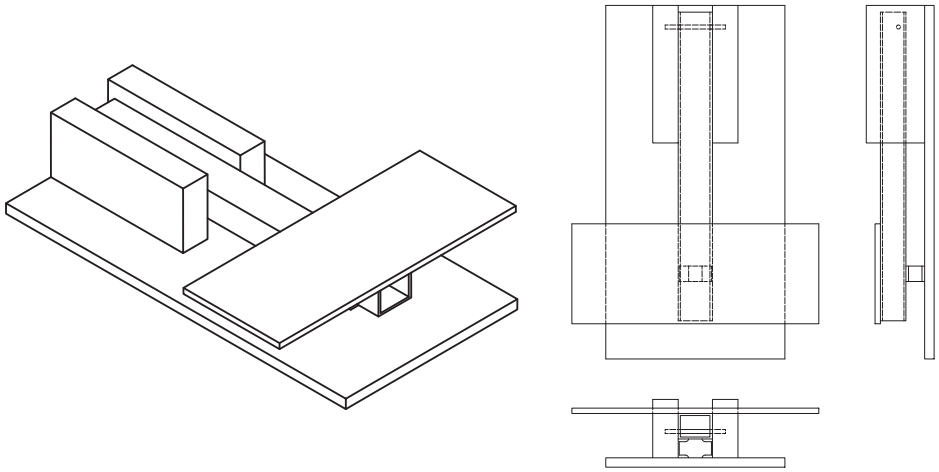

Figure 5.2: Diagram of force plates used to detect reaction force at each of the feet.

The three Transducer Techniques MLP-300 load-cells each contained a standard strain gage Wheatstone bridge circuit. The load cells have a rated output (RO) of 2 mV/V, a nonlinearity of 0.1% of the RO, hysteresis of 0.1% of the RO, non-repeatability of 0.05% of the RO and a zero balance of 1.0% of the RO. The load cells are rated for loads of up to 300 lbs (136 kg, 1335 N). With an excitement voltage

of 10 VDC, the output of each sensor was amplified and read via a USB NI DAQ analog to digital converters. Using MATLAB's Data Acquisition toolbox, the three voltage signals could be read and recorded at 100 Hz. For each force plate, known masses were used to create a calibration curve. The linear relationship between the raw output value of the load-cell and the known mass applied was used to derive an offset value and a scaling factor for converting raw load-cell values into units of kilograms.

To efficiently record and organize the force data obtained, a MATLAB program and GUI were designed to allow for intuitive and efficient user input and well-managed data output. The GUI, seen in Figure 5.3, allows for a one-click tare of the signals and simple recording. The visual output to the user consists of numerical readouts, in kilograms, for each of the three sensors, and a scrolling plot that shows the real-time readings from the load-cells. The *name* and *date* fields are input by the user of the software and are used to name the text files in which each set of data is saved. The *test* field is also used in the naming of the saved data. This field, meant for the consecutive integer number of the test, can be input by the user and increases by one automatically after a set of data is recorded. This feature avoids the accidental overwriting of existing data. A press of the record button creates a file using the name, data and test number found in the fields. The program writes the timestamp (in seconds) and force sensor data (in kilograms) to the file at 100 Hz until the stop button is pressed. The file is closed and the test number increases automatically by one. To record the next test, the user simply pushes record again.

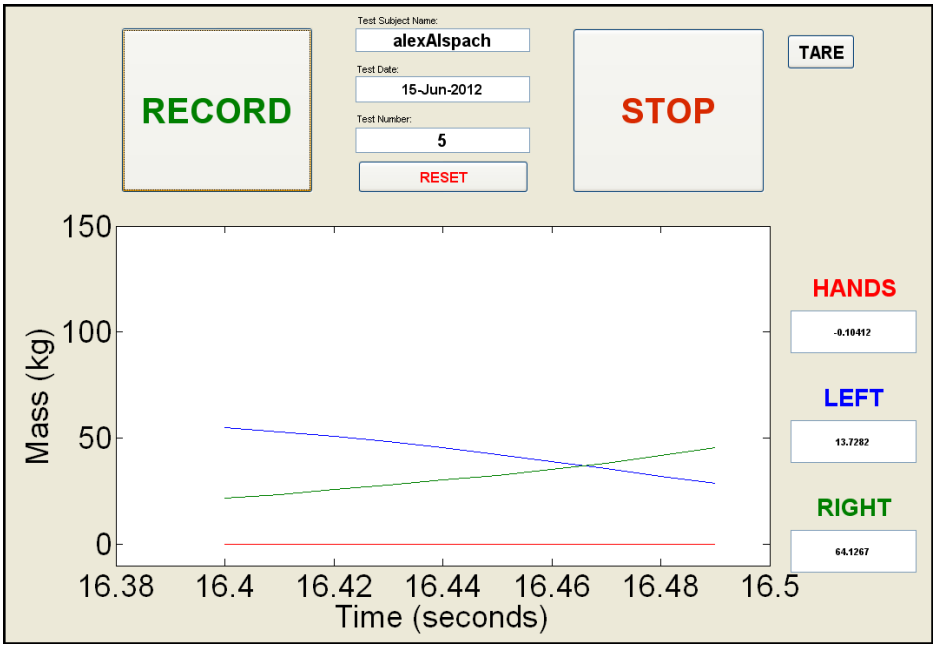

Figure 5.3: MATLAB GUI designed for quick and easy data logging and management

5.1.2 Procedure

The motions and forces produced when pushing a static object were recorded for seven males of medium build with the feet together and for five different posteriorly displaced back foot locations: 0, 20, 40, 60, 80 and 100 cm. Subject ages ranged from 19 - 28 years with a mean of 23.9 years and a standard deviation of 3.5 years. For this group, the mean mass is 74.3 kg (standard deviation: 15.1 kg) and the mean height is 175.4 cm (standard deviation: 5.9 cm).

Each subject wore a motion capture suit with 34 reflective markers throughout all experimental tests. The locations of these markers were adjusted to each subject's body. For each subject, a rigid body skeleton was designed and fitted to the subject using the motion capture software. Once fitted, this skeleton could be used to track the body motions and joint locations within the visible motion capture area. This

rigid-body skeleton could be saved and reloaded for use during later testing.

For each subject, two main pushing experiments were conducted with one fundamental difference: In one, the subjects were asked to keep their upper-body in line with their extended back leg. In the other, the upper body was allowed to rotate relative to the back leg. The aligned upper body and back leg test was meant to represent a single inverted pendulum model while the unconstrained experiment would represent more natural methods of pushing.

The experimental setup consisted of a fixed, vertical box. Attached to the side of this box was a force plate that would detect the horizontal, positive x-direction force exerted by the subject at the hands. The force plate was fixed to the box with hook-and-loop fastener so that it could be easily removed and reattached at varying heights. On the floor were two more force plates used to measure the vertical, negative z-direction forces transmitted to the floor through the subject's feet. These force plates were also attached with hook-and-loop fastener and could each independently be placed and fixed at varying distances from the pushing plane. This allowed for feet-apart poses of varying lengths to be tested. The force plate setup used for push testing can be found in Figure 5.4.

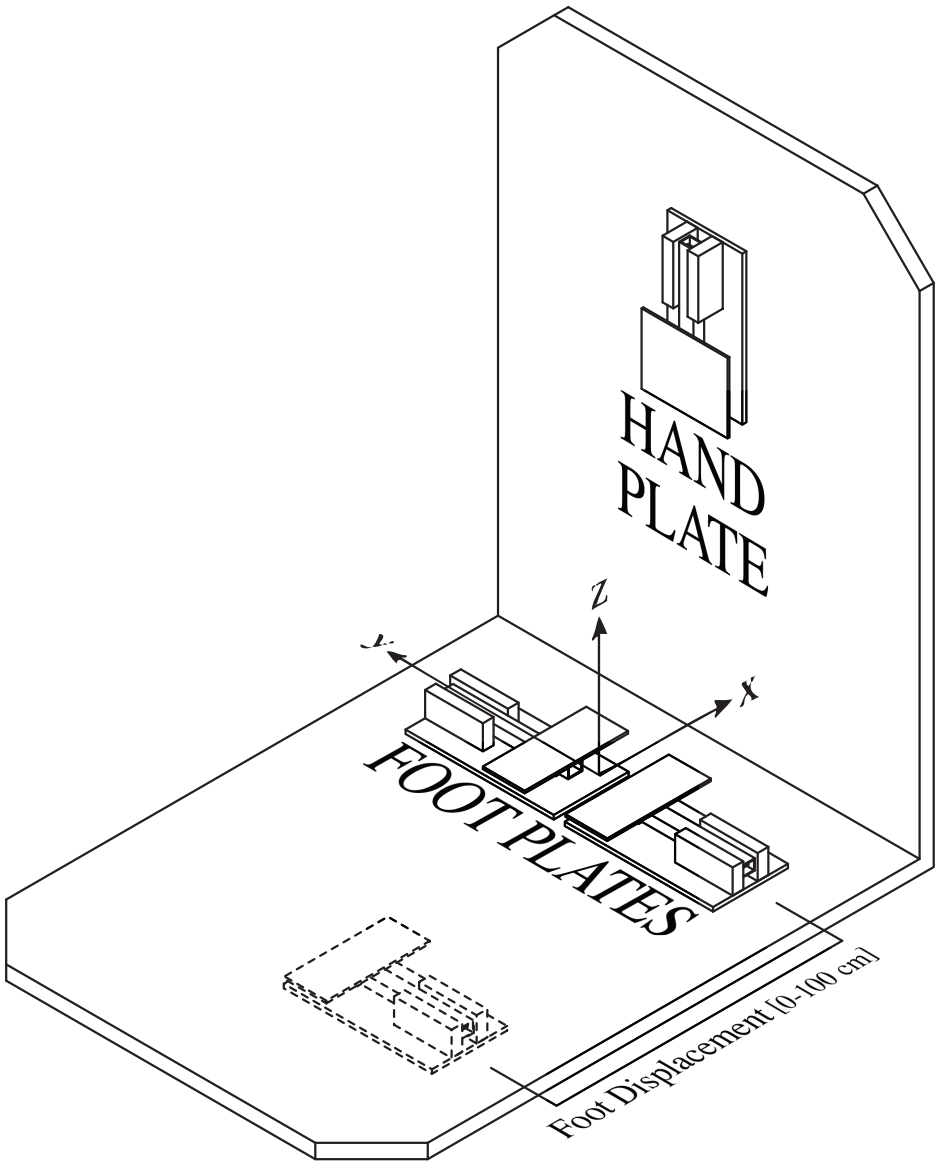

Figure 5.4: Diagram of force plates set up for pushing tests with motion capture origin in place. The dotted-line force plate at the rear represents the extent of rear foot displacement during testing (1 m).

Upon starting the test, the subject was asked to push on the box (without a force plate) with one foot back so that a natural pushing stance could be determined. The distance from the pushing plane to the middle of the front foot was measured for use when placing the force plates. The foot naturally chosen as the rear foot was also noted.

The foot force plates were attached to the floor with their geometrically centric load-cell placed at the subject determined distance from the pushing plane of the now-attached hand force plate as in Figure 5.4. The subject was asked to stand on the force plates so that their symmetric distance from the subject's sagittal plane could be adjusted to allow for a natural foot distance along the sagittal axis. The feet should naturally settle with the estimated center of pressure of each foot being in the center of the force plate. For each subject, two ten-second readings of foot force data with minimal body movement were recorded. This data was summed and averaged to obtain the subject's mass.

The experiment proceeded as follows, the subject was asked to step onto the aligned force plates and the center of the hand force plate was adjusted to shoulder height and aligned to the subject's sagittal plane. The subject was asked to assume a statically stable pre-pushing posture with hands out but not contacting the hand force plate. At this point, the logging of both the force and motion data was started. The subject would then push on the force plate five times, exerting the maximum force they could in that pose and assuming the same stable no-hand-contact pre-pushing stance between each push. The subject was asked to push using only horizontal force while avoiding sudden motion and impulses. After each set of five pushes, the recording was stopped. The subject was asked to step off of the force plate then step back on to more randomize the force error caused by eccentric foot placement. A second test in the same stance was then conducted and recorded.

After two tests in a given pose, the force plate under the subject's favored rear foot was moved back by 20 cm, reaffixed to the floor using the hook-and-loop fastener,

and two more sets of five pushes were recorded. Six stances were tested with ten total recorded pushes each. The feet were displaced by 0, 20, 40, 60, 80, and 100 cm. The set of 12 total tests was performed twice: once for the aligned back leg and upper body (IVP) and once with a free-to-articulate waist (DIVP).

As the posterior foot displacement became larger, adequate friction became more necessary when pushing. To avoid foot slippage as a variable, the force plates were sprayed with high tack spray glue to create a sticky, high friction surface. The hook-and-loop fastener did an adequate job of keeping the force plates in their intended locations without changing position or orientation. The experimental constraints imposed upon each subject during testing were:

- The front foot must remain in the initially selected position throughout the experiment, effectively eliminating its location as a variable
- The back leg must remain fully extended throughout all tests
- The center of pressure of each foot must be maintained at center of force plate for all tests
- The hand force plate must be adjusted to shoulder level for pre-pushing stances at each feet-apart stance length
- Subject must avoid impulses to the force plates

5.2 Data Analysis

The data collected, both from the motion capture system and from the force plates at the feet and hands, is not intended for direct application to the humanoid robot. Instead, this data is used to explore the applicability of the linearized double inverted pendulum model over the more simplified and more limited single inverted pendulum

model used in previous humanoid pushing research. The importance of one foot placed up front during pushing is also of great interest.

With the constraints on foot placement mentioned in Section 5.1, the mass distributions for stances assumed prior to and during pushing were studied. To fully appreciate the benefits of the feet-apart stance chosen for testing, we must first address the limitations when pushing with one's feet together. If one intends to push using this feet-together method and some great body angle, there are two ways that this stance can be assumed: the person can fall onto the object being pushed, catching oneself with the hands, or stability can be found with a foot forward, then, once the hands are in place, the front foot can be moved back to meet the other. In this stance, a human may be able to produce substantial force but is only able to modulate this force minimally. Further, the pusher relies on the object for stability and will likely fall if a sudden movement of the object occurs.

In [1], this ability to modulate the force at the hands while in this feet-together stance (Figure 2.1 on page 5) is examined using a single inverted pendulum model Figure 5.5.

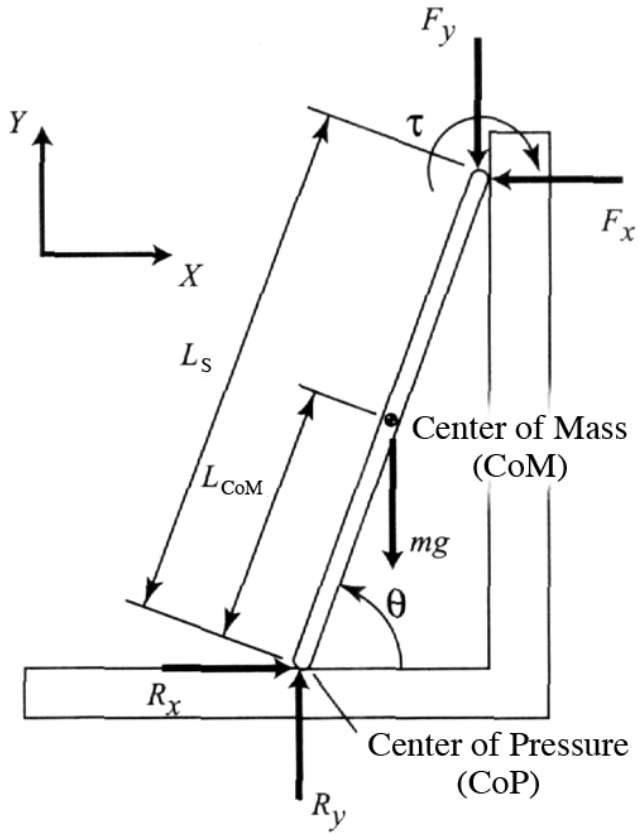

Figure 5.5: Single inverted pendulum model of a human pushing with point contact. Adapted from Rancourt and Hogan,"Dynamics of Pushing", 2001. [1]

The moment balance equation about the link-ground contact point for this inverted pendulum model in static equilibrium is:

$$M_{CoP} = F_x L_S \sin(\theta) - mgL_{CoM}\cos(\theta) - F_y L_S \cos(\theta) - \tau = 0, \tag{5.1}$$

where F_x is the horizontal component of force between the hands and the pushing plane and F_y is the vertical component, m is the body mass, g is the acceleration due to gravity, L_{CoM} is the distance along the link from the point of ground contact to the center of mass, L_S is the shoulder height, θ is the angle of the link relative to the horizontal axis and τ is the moment between the hands and the pushing plane. Since

we are interested in the horizontal force applied by the hands to the pushing plane, the equation can be rearranged as follows:

$$F_{hands} = F_x = mg\frac{L_{CoM}}{L_S}\cot(\theta) + \frac{\tau}{L_S \sin(\theta)} \tag{5.2}$$

From this equation, it is evident that the horizontal force can be modified via a change in gravity or a hand-exerted vertical force, change in mass of the body, an application of torque at the hands or a change in link length from the point of ground contact to the body's CoM. While the vertical forces due to the body's mass will remain constant, torque and vertical force at the hands will be considered negligible. This leaves the modification of the pendulum angle or the location of the CoM along the link for varying the horizontally applied force. The angle of the body link can be changed dramatically by a changing of the foot distance from the pushing plane, or, within a chosen stance, can be changed within a small range via extension and flexion of the arms. Assuming that the angle chosen initially is kept constant, one of the two supporting legs can be extended forward (without contacting the ground) or raised up along the body to heighten the CoM and increase the force exerted at the hands.

Rancourt and Hogan have estimated that the maximum pushing range via raising of the CoM (by concentrating the mass of one leg at the hip), using the application of vertical force and of applying torque at the hands in [1]. Using anthropometric values from Kroemer et al. [32] and Chaffin and Andersson [33] for an average male, the maximum pushing range for a body tilt angle of 10 degrees is 6 N via raising of a lower limb, 19 N via vertical force at the hands and 7 N via a torque applied at the

hands. For a 20 degree angle from vertical, an 11 N range can be obtained by raising of a lower limb, 37 N via vertical hand force and 7.4 N via an applied torque at the hands.

The inverted pendulum model simplifies the feet down to a point of contact, when, in reality, the feet contact the ground on a finite surface. While small variations in force can be produced using other methods, varying forces can also be produced when the position of the body's ZMP can be shifted within the support polygon. For the feet-together pose, this support polygon is small, but allows the ZMP to be moved forward to the toes prior to pushing. From an upright position, and with an estimated 15 cm-long foot, the single-link body is able to lean forward about 8 degrees [1]. This pre-push shift creates a larger margin for ZMP while pushing by bringing it to the front of the support polygon, allowing a larger force to be exerted at the hands before instability is realized. Stability is lost when the ZMP exits the support polygon at the rear. Rancourt and Hogan calculate the pushing range using this shift of ZMP location to increase to about 77N [1]. This is compared to standing straight up and pushing with a simulated point contact and no allowable ZMP movement.

This ability to preset the ZMP at a far-forward location can truly be exploited when in the feet-apart stance with one foot forward, supporting most of the weight, while the other is set back, prepared to take the load when pushing. In this stance, the ZMP should start towards the front of the elongated support polygon and move back as the force increases at the hands. Rancourt and Hogan calculated the maximum force in this stance to be on the order of 655 N (with the extended back leg and aligned upper body at a 50 degree angle off of vertical) for an average-size male [1].

While, theoretically, this stance should produce about the same maximum force as a feet-together pose at the same angle (and stabilized by the unmoving pushing plane), the major benefit lies in the ability to stably assume the position then control the amount force at the hands (between zero to some maximum force).

In exploring these characteristics of the feet-apart pose, Rancourt and Hogan, like Harada, Stilman, Motoi and Hwang, only considered a single inverted pendulum model of the human body. With the rigid constraint at the waist removed but foot placement and shoulder height kept constant, coronal axis translation of the hips becomes available to the pusher. With the benefit of the feet-apart stance established, the effects of this ability to move the CoM with this stance warrants investigation. Human motion and reaction force analysis was conducted to determine the use of waist, and whether or not this motion allowance is advantageous for use on a humanoid robot in the pushing of an unknown mass.

5.2.1 Reaction Forces

The first question to be answered was whether or not a human could produce a larger force when waist articulation was allowed versus if he was constrained to maintaining alignment of the extended back leg and upper body. As stated in Section 5.1, tests were conducted with and without this single IVP constraint. It was found that, with the ability to bend at the waist, more force could be produced at the hands. The four plots seen in Figure 5.6 represent the mean value of four subjects' reaction forces at the hands with rear foot displacements ranging from zero to 100 cm from the front foot. The exerted force data per foot displacement for each subject is normalized

by dividing each displacement by the subject's shoulder height [29], providing an independent variable that is proportional to the size of the subject. This technique assumes that the strength, as well as the geometry of the legs, is proportionate to the subject's upright-standing shoulder height. Second-order polynomials are used to find an estimated maximum difference in force at the hands for an IVP and DIVP push. For subject 1, the maximum difference in force exerted using DIVP-style body motion over the constrained IVP motion is about 112 N. The mean increase in force over all of the different foot placements is 85 N. For subject 2, the maximum difference in force at the hands is 96 N with a mean difference of 52 N. For subject 3, the difference comes to 63 N with a mean of 34 N and for subject 4, the maximum difference is 110 N with a mean of 94 N over all foot placements. DIVP pushing versus IVP pushing for all subjects has an average pushing force difference over all poses of 66 N. While the data shows that more horizontal force is able to be applied when allowing motion at the waist, it is worth noting that these differences only fall somewhere in between full waist motion allowance and a straight rigid body from ankle to chest. While testing the IVP pushing, subjects complained of discomfort and inability to easily maintain the constraint while pushing. It became evident that this posture is far from a natural pushing stance, supporting the exploration as to why.

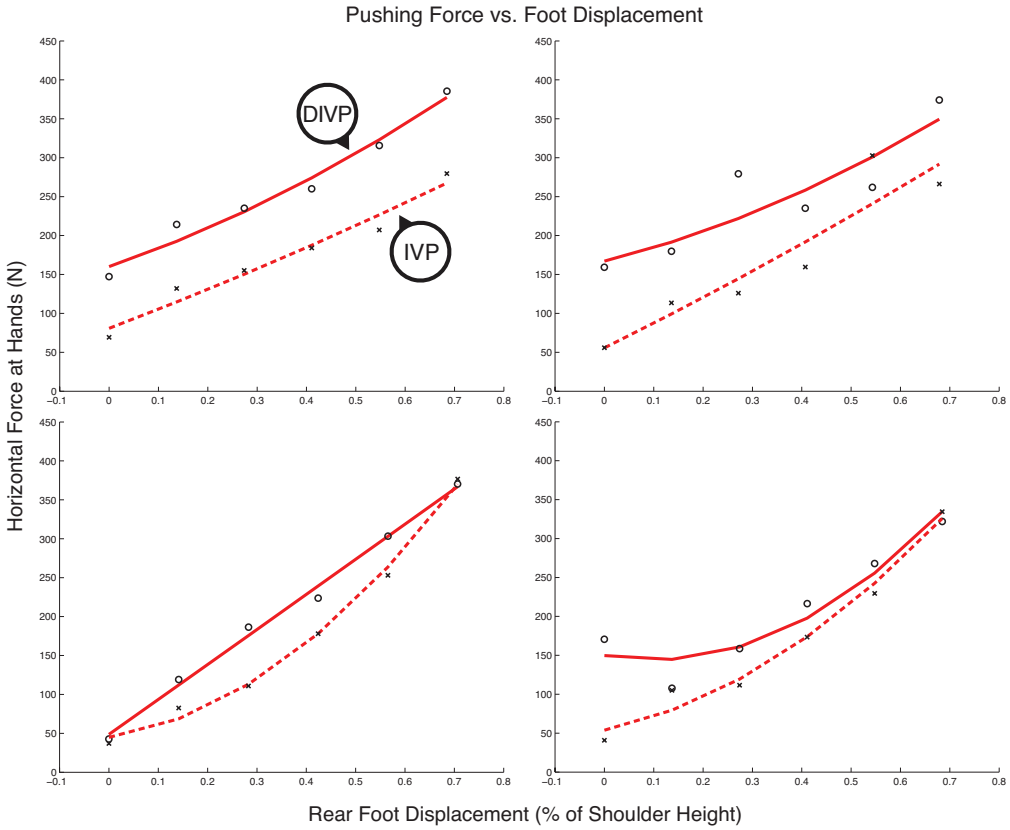

Figure 5.6: Pushing force data for four subjects shows the difference in force exerted at the hands over all tests with and without the IVP motion constraint.

Allowing the subject to push at their own pace, strict timing of the pushes was not enforced. The force data obtained was relatively consistent in magnitude, but did not necessarily adhere to a periodic cycle. Furthermore, the force curves produced often varied in shape due to uncontrollable differences in pushing abilities or methods and other uncontrollable variables. Even for tests of the same subject, curve shapes and push timing varied greatly enough between tests to make the automated dividing of pushing and non-pushing reaction forces a difficult task. These characteristics can be seen in Figure 5.7 where two pushing tests of the same subject are presented for comparison of periodicity and curve form. To maintain consistency throughout all

data analysis, a simplified method of calculating the average reaction forces at the hands and feet while in the statically stable pre-pushing stance and while exerting the pushing force was adopted. Because both the stable pre-pushing stance and the stance when exerting the pushing force were held for a few seconds at a time, visible plateaus with steep slopes up and down emerged when plotted over time. Loosely resembling a square curve, the reaction force at the hands was most commonly at about zero or at some maximum pushing force for a given test and spend little time in between. Because of this characteristic, the maximum pushing force at the hands for each test was considered the mean of the data above the total mean hand force for each test. Hand force values above this mean indicated the time periods during which the subject was considered to be pushing (Figure 5.8). For both the front and rear feet, the reaction force data falling within these pushing time-periods was averaged to find a mean pushing z-direction reaction force for each foot. The data falling within the time periods during which the subject was not pushing were used to calculate mean foot reaction forces for the static pre-pushing stance. While this method causes underestimation of the maximum and minimum magnitude, it is sufficient for displaying the characteristic trends in force exerted and corresponding ground-foot reaction forces as the length of the support polygon is varied.

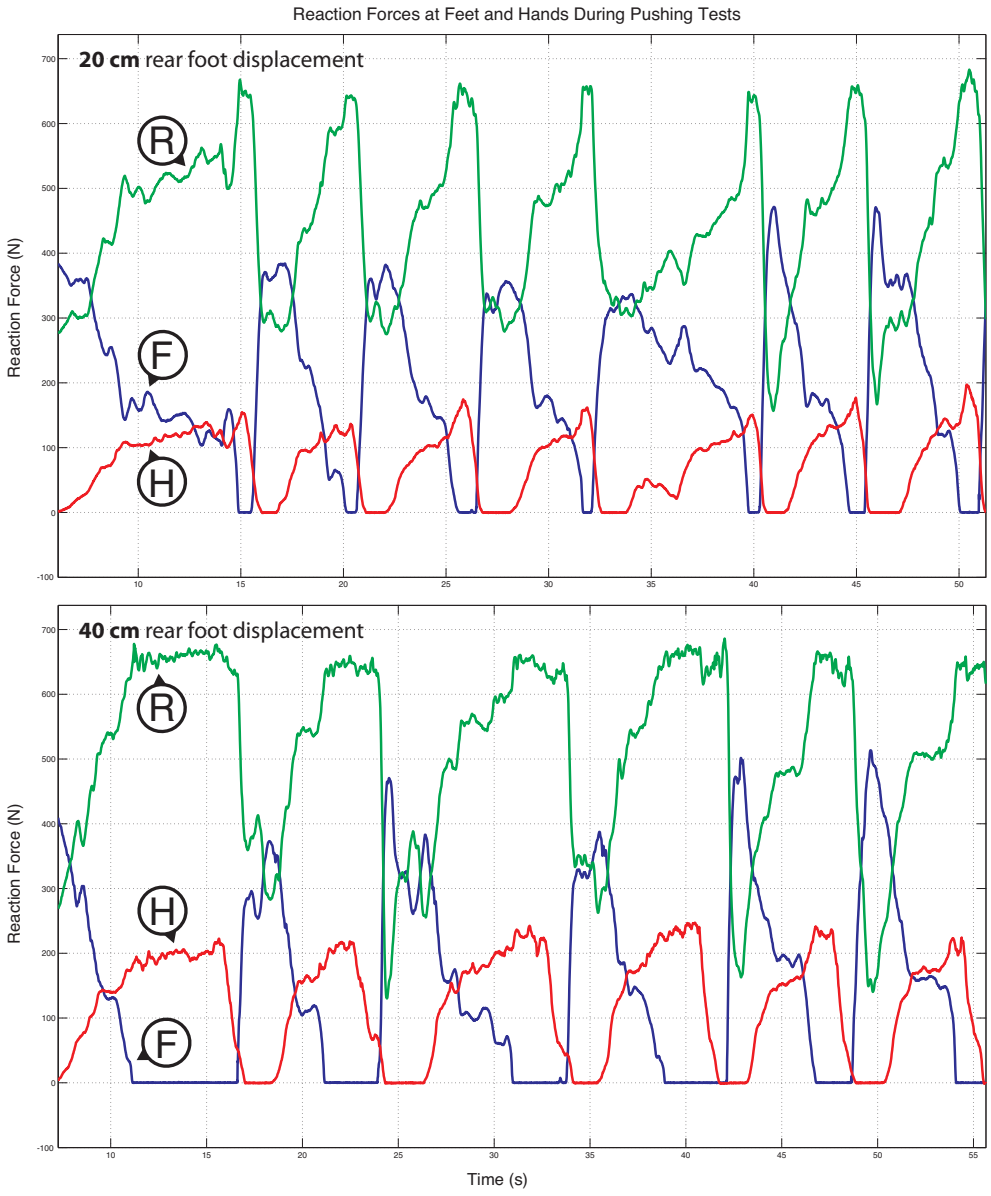

Figure 5.7: Reaction force data can vary greatly in periodicity and shape characteristics, even for tests of the same subject. H, R and F represent the reaction forces at the hands and the rear and front feet, respectively.

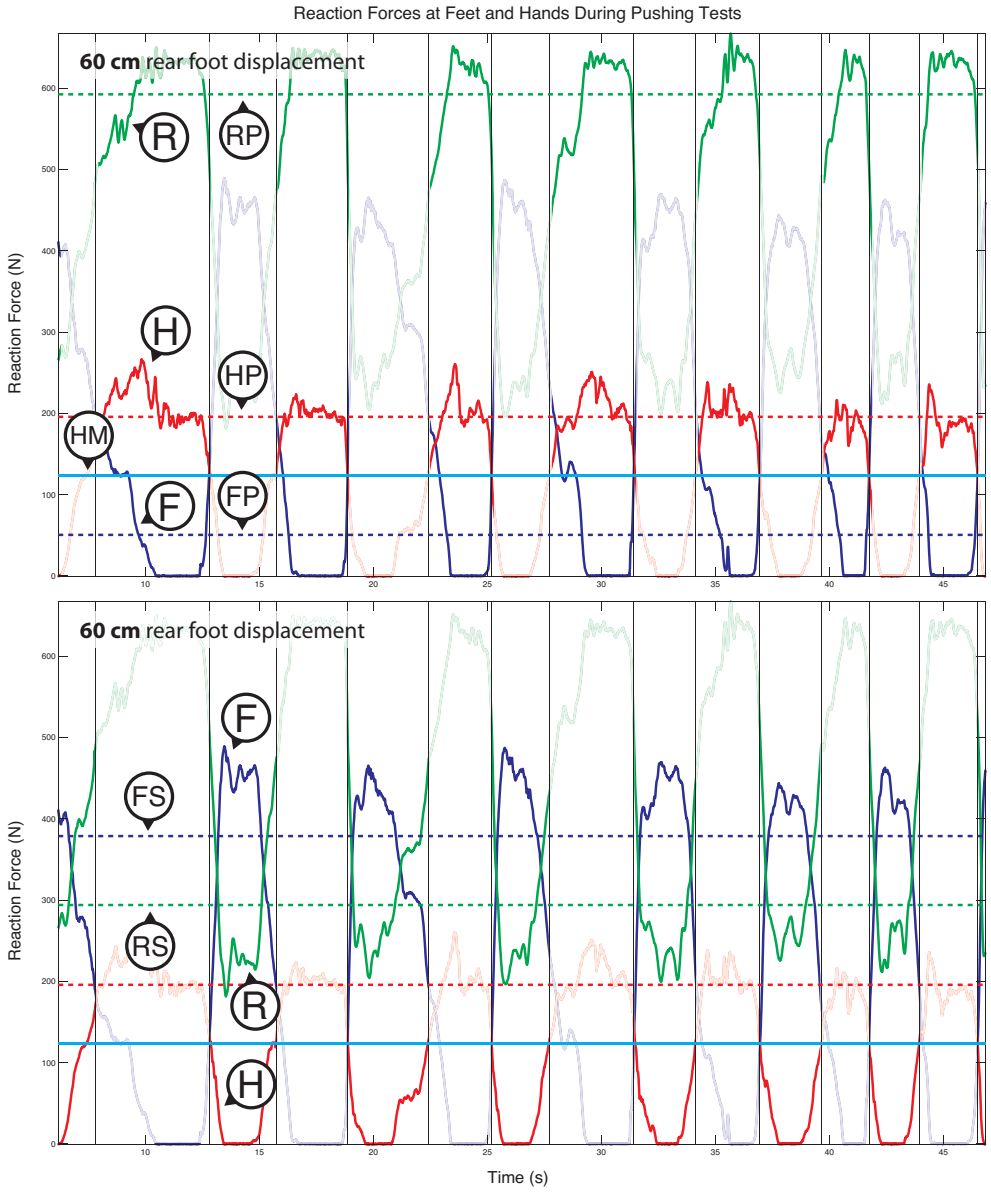

Figure 5.8: Time periods where the force at the hands fell above and below the mean of the total hand force data set were considered periods of pushing and pre-pushing, respectively. The pushing time periods (**top**) and pre-pushing periods (**bottom**) are shown in the plots above where *H*, *R* and *F* represent the reaction forces at the hands and the rear and front feet, respectively. *HM* is the total hand force mean, *RP* and *FP* are mean **pushing** reaction forces at the rear and front foot, respectively, and *RS* and *FS* are the mean **pre-pushing** reaction forces at the rear and front foot, respectively. *HP* represents the average pushing force exerted at the hands.

As established in Chapter 4, analyzed statically, the x-axis ZMP of the pushing body at any point in time can be calculated as the coronal-axis center of pressure. The ZMP location can therefore be estimated using the force distribution at the feet, i.e. the ratio of the vertical force at each foot with respect to the subjects weight. This one-dimensional ZMP, located between the separated feet when statically stable, can be calculated as follows:

$$\frac{F_{F,z}d_{F,x} + F_{R,z}d_{R,x}}{mg} = ZMP_x, \tag{5.3}$$

where $F_{F,z}$, $F_{R,z}$, $d_{F,x}$ and $d_{R,x}$ are the reaction forces and x-direction locations of the the front and rear feet, respectively. m is subject mass, g is the acceleration due to gravity, and ZMP_x is the location of the ZMP on the x-axis. The coordinate system used for these calculations can be found in Figure 5.4.

During a push (Figure 5.9), the movement of the ZMP location between the displaced feet can be realized. While in the stable, pre-pushing stance, this point is located between the center of the stance and the front foot, indicating that the front foot is supporting most of the subject's body weight. When the maximum force at the hands has been reached, this point is located at the back end of the support polygon, i.e. the back of the rear foot. The ZMP's location at this rear boundary of the support polygon indicates the instability (tipping) of the body and the upper limit of force produced at the hands. In most tests, the absence of force on the front foot (as seen at point 2 in Figure 5.9) does not indicate instability, but rather a ZMP location further forward on the rear foot. It is natural to lift the front foot up during

the exertion of large forces at the hands for two reasons: Applying any force on the front foot creates a moment that counteracts the pushing force [29] and, if raised and/or moved anteriorly, the mass of the suspended leg will increase the amount of force able to be exerted at the hands [1].

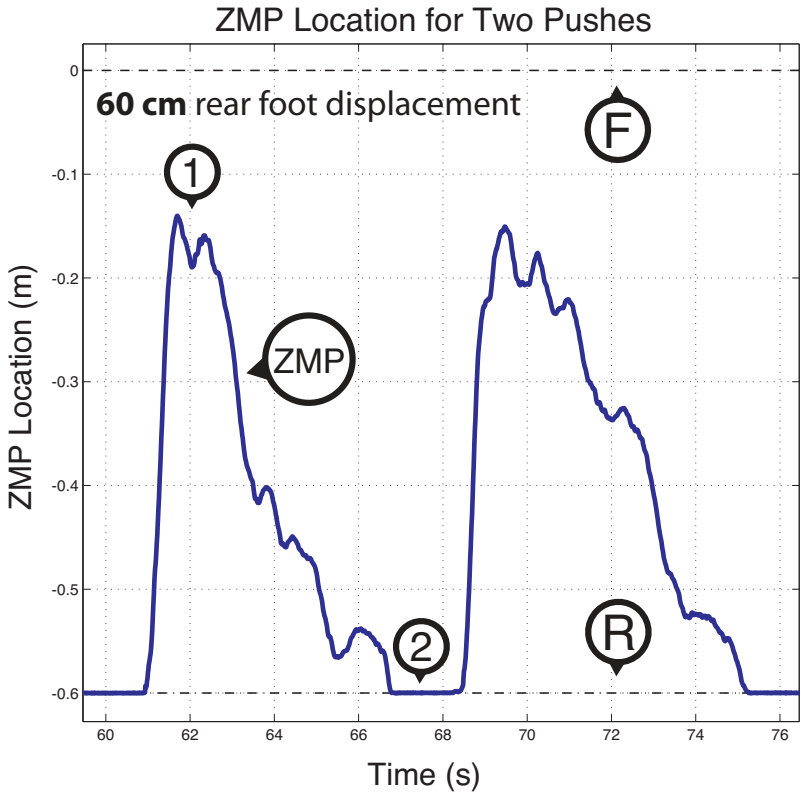

Figure 5.9: ZMP location change during two pushes. F and R correspond to the front and rear foot locations, respectively. Points 1 and 2 show the ZMP location for the pre-pushing pose and at maximum hand exertion, respectively.

Generally, during DIVP pushing, the subject assumed a statically stable pre-pushing stance with the ZMP location further forward than for the IVP pushing. The ZMP's changing of locations over a five to seven push test can be seen in Figure 5.11 for both the IVP and DIVP pushes at foot displacements of 20, 40 and 60 cm. These three displacements were chosen to exemplify this change in available ZMP margin

because they fall in the middle range of the six displacements tested. These mid-range displacements represent the most comfortable and most likely positions to be chosen by the subject when freely pushing (as noted by the subjects). For the subject whose ZMP plots are shown in Figure 5.11, the maximum difference in how much further forward the subject could position the ZMP prior to pushing when able to move at the waist is about 3.5 cm with a mean of about 2 cm (Figure 5.10). Across all subjects tested with the IVP constraint, the mean difference in ZMP location between the IVP and DIVP-style pre-pushing stance is about 1.8 cm further forward for the DIVP push with a standard deviation of 0.39 cm.

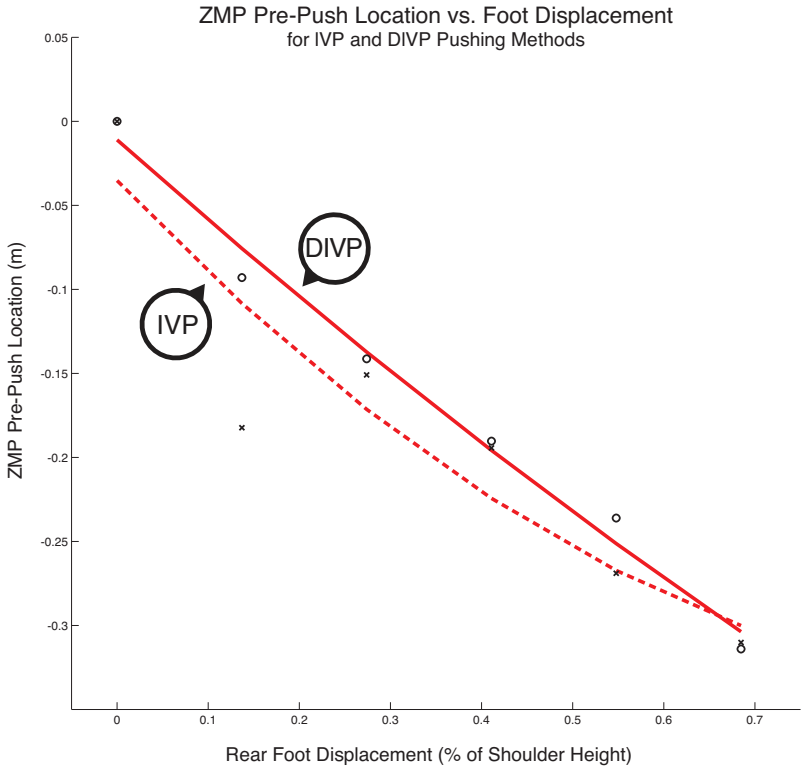

Figure 5.10: ZMP pre-push location difference for all tests of IVP and DIVP-style pushing of the subject in Figure 5.11.

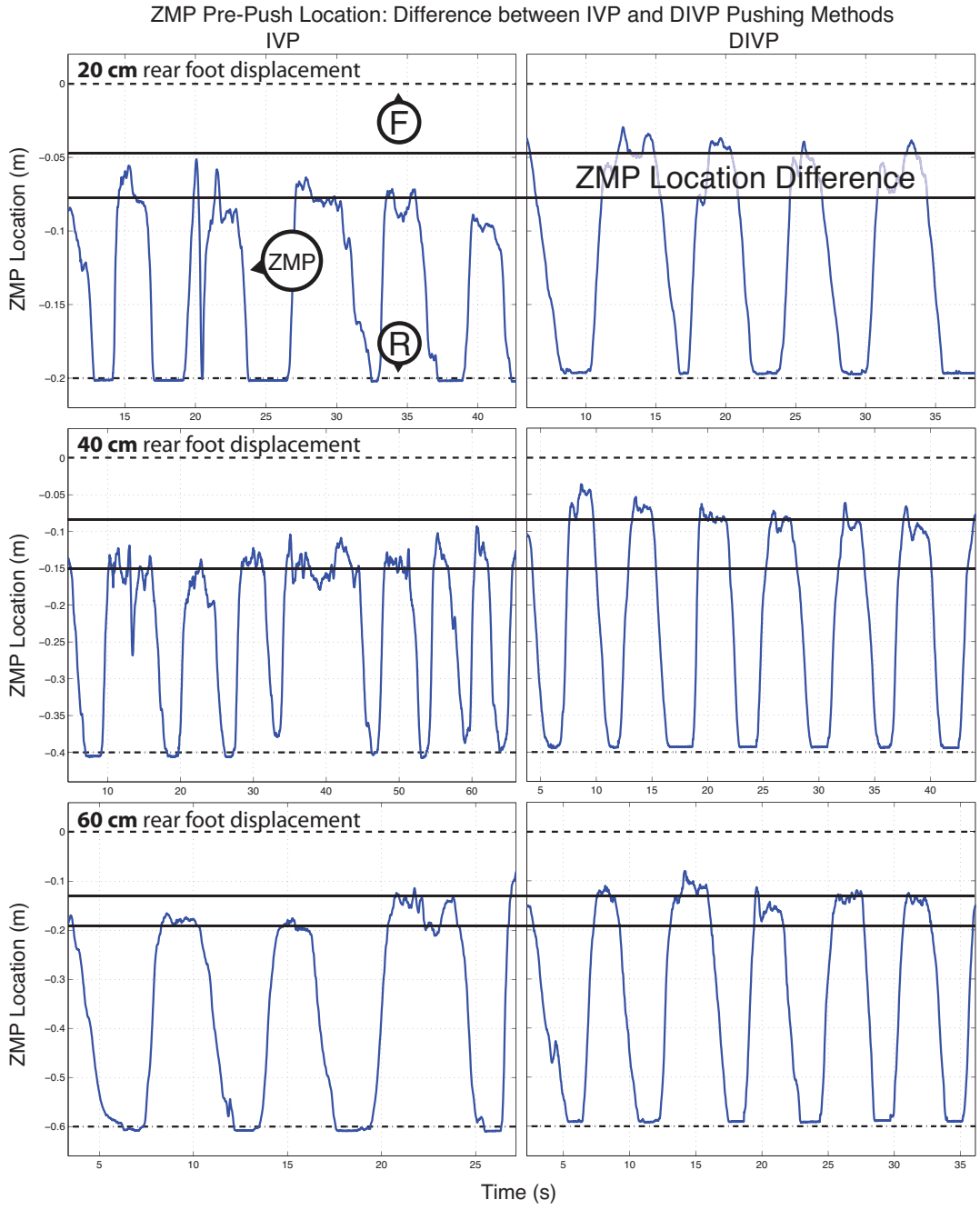

Figure 5.11: ZMP pre-push location difference for 20, 40 and 60 cm tests of IVP and DIVP-style pushing. F and R correspond to the front and rear foot locations, respectively. Solid black lines indicate the mean pre-pushing ZMP for both IVP and DIVP pushing for each stance width.

With the ZMPs limit always at the back of the posteriorly displaced foot, setting the ZMP as far forward as possible before pushing increases the overall amount of force able to be exerted before tipping backward. It can be seen in Figure 5.12 that when the ZMP distance from the front foot is a smaller percentage of the total stance length, greater pushing forces can be exerted. Allowing the subject to move at the waist provides the ability to set the ZMP further forward than if they are constrained to keep their upper body aligned with their extended back leg. With constraints only on foot placement and pushing location, the joint angles of the body can be modified to bring the CoM, and therefore the ZMP, forward prior to pushing when waist articulation is allowed. Motion capture analysis of the body during these tests was conducted to see how each subject reoriented their body links produce this observed shift forward of the ZMP.

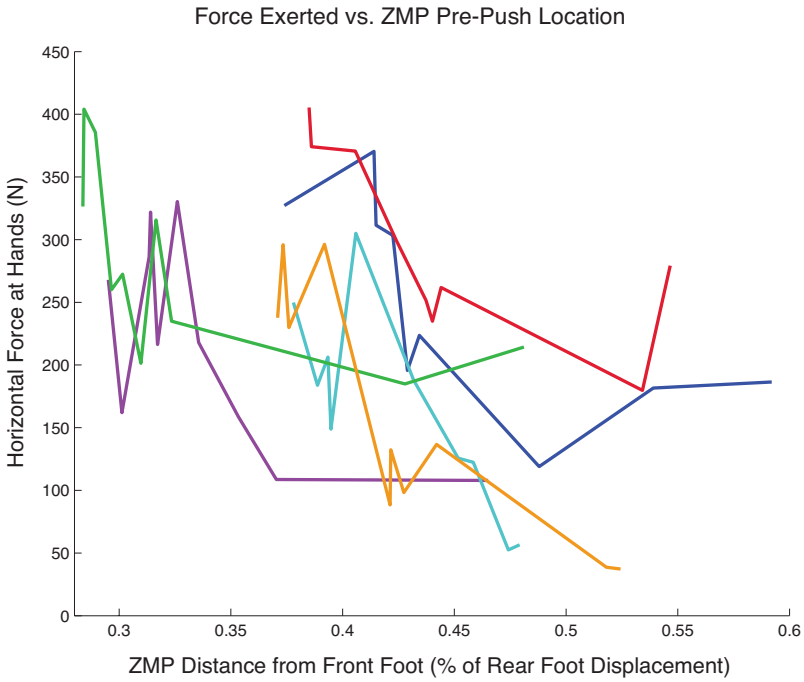

Figure 5.12: Pushing force versus ZMP pre-push distance from front foot as a percentage of total stance length. Data plotted for all subjects.

5.2.2 Joint Angles

For each pushing test, the three-dimensional locations of each joint on the subject's body were recorded using a motion capture system. For two-dimensional analysis, the coordinate system used considered the positive x-direction as forward with respect to the subject. The positive z-direction points upward with zero on the foot-force plate plane. For the leg, joint locations were obtained for the ankle, knee and hip joints. The locations of the ankle and the hip were used to calculate the angle of the simplified extended back leg with respect to vertical. The ankle angle is considered zero when the link is vertical (standing) and adheres to a right-handed convention with a positive clockwise (forward) rotation. For the upper body, three-dimensional locations are recorded for the waist, abdomen, chest and shoulders. The upper body was simplified into a single link using the hip and shoulder locations and used to obtain the angle of the upper link. This link follows the same right-handed sign-convention for rotation as the lower link.

The motion capture system records the subjects movements at 100 Hz and outputs every joint location for each frame. The link simplification and angle calculations were performed for each frame. Each set of data contains the body motion for a test with five or more pushes. The oscillating angles of the upper and lower body links were plotted over time and decomposed into the mean link angles during pushing and during the stable pre-pushing stance. As with the force data, these oscillations were not necessarily periodic nor were the amplitudes consistent. It was therefore necessary to decompose these angles in the same way as the hand force. For each link, the mean

angle was found using the data set for the full, multiple push test (Figure 5.13). The mean of all data points that fell above the total data sets mean was considered the maximum angle for each link. The minimum angle was considered to be the mean value of the data below this total mean. This estimation method was used for both the upper and lower body links to obtain a single value for each link's pushing and pre-pushing angles. Although this method underestimates the extreme values, these angle estimates were considered sufficient for subsequent analysis and consideration. It was determined by inspection that the estimated maximum angle for the lower link corresponded to that link's angle while pushing and the minimum angle for the upper link was its angle while pushing. The maximum angle for the lower link therefore corresponds to the stable, pre-pushing stance, as does the maximum angle for the upper link.

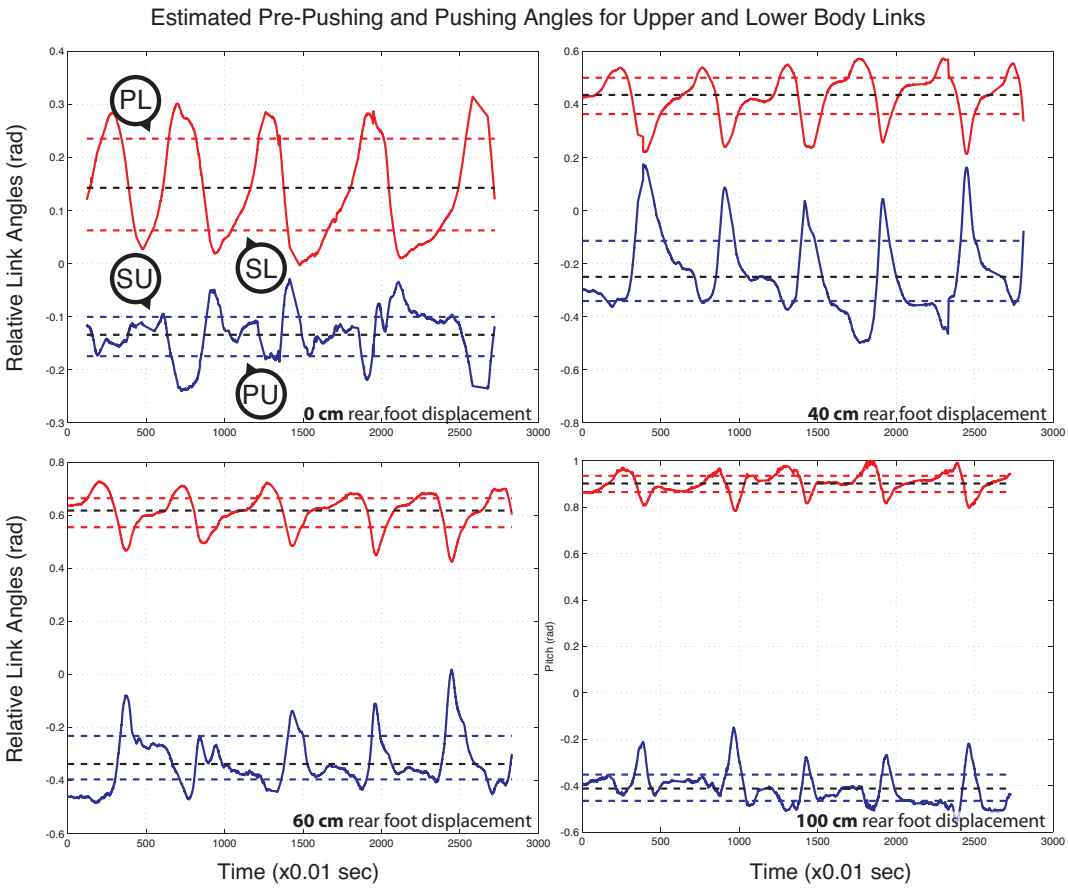

Figure 5.13: Estimation of mean relative angle (rad) for a subject in the **S**table pre-pushing stance and while **P**ushing for the **U**pper and **L**ower body links: *SU*, *SL*, *PU* and *PL*, respectively.

It was found that, when pushing an unmoving object, subjects generally performed the task in the same way, resulting in a good understanding of how a human is able to maximize the ZMP displacement margin before pushing. As in all tests, the pushing force plate was adjusted to the shoulder height of the subject for each stable pre-pushing stance. Once chosen, the shoulder height became constrained throughout the test at each foot displacement. The pusher managed to locate the ZMP as far forward as possible by rotating the upper link about a global point not coincident with the waist. This motion effectively pushed the hips forward while maintaining

the original shoulder height within a few vertical centimeters. When possible, as in the less widely displaced-foot poses, The upper body wound up almost vertical as the subject pushed. As the stance got wider, arm reach became a limiting factor, along with hip, knee and ankle flexibility. The subjects still attempted to push the hips as far forward as possible without drastically lowering the shoulders. This observed pushing technique was confirmed through two-dimensional analysis of the motion capture data (Figure 5.14). These two-dimensional diagrams can be compared to the motion capture software rigid-body skeleton representation of the joint configurations when positioning and pushing (Figure 5.15)

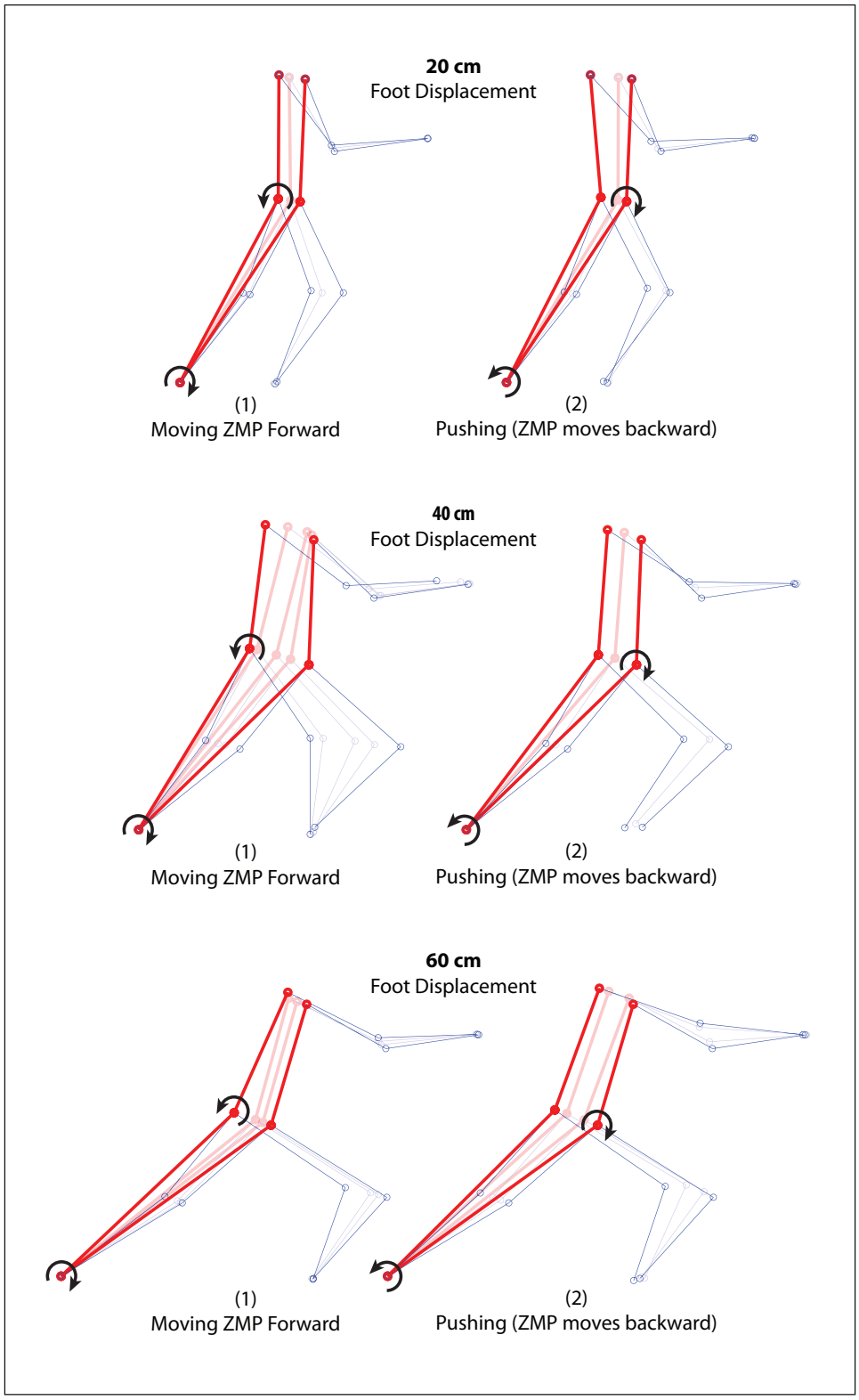

Figure 5.14: Rotation of the unconstrained upper body link to move ZMP forward when pushing an unmoving object.

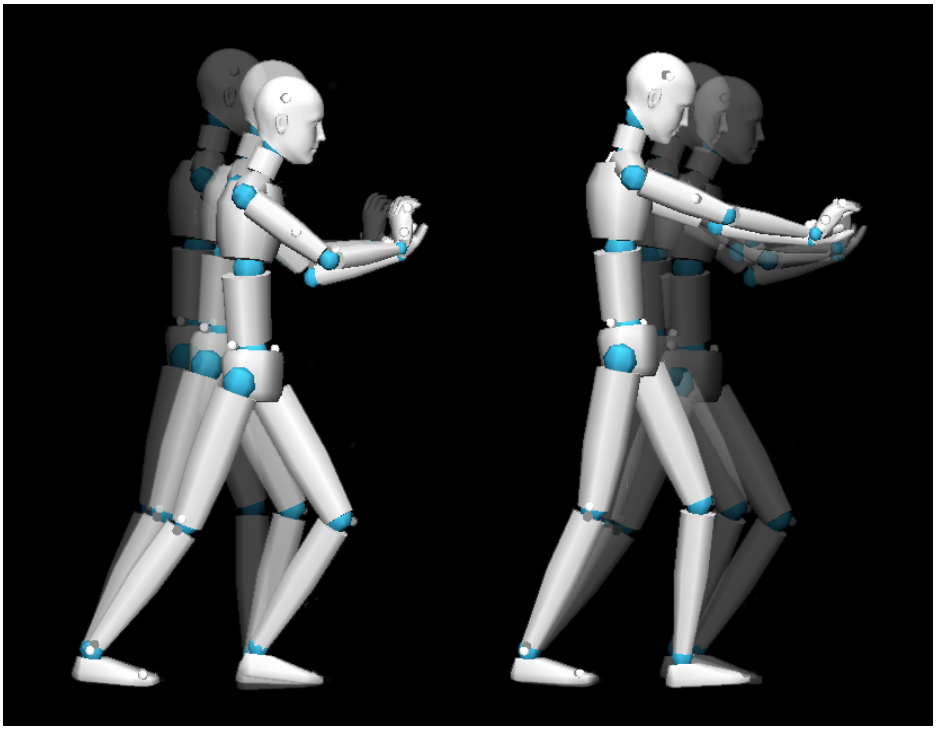

Figure 5.15: Motion capture skeleton during the pre-pushing ZMP forward movement (**left**) and during pushing (**right**) for a 40 cm foot displacement.

When in a feet-apart stance and exerting maximum horizontal force on a static object, the ankle angle varies linearly with the distance between the rear and front feet (Figure 5.16). This angle, measured from the vertical axis, is considered positive when leaning forward. The pre-pushing ankle angle, although slightly less (on the order of 5 degrees less), also follows a linear trend and increases in angle at about the same rate for changes in foot displacement. The waist angle, or angle between the extended back leg and the upper body, follows a decreasing linear trend as foot displacement increases. Following the same convention as the ankle joint, this angle is negative as the upper body is bent backward relative to the legs. Again, the upper link angle decreases at about the same rate for the pre-pushing and the more negatively angled pushing stances with the difference between them being on the same order as

for ankle angle difference.

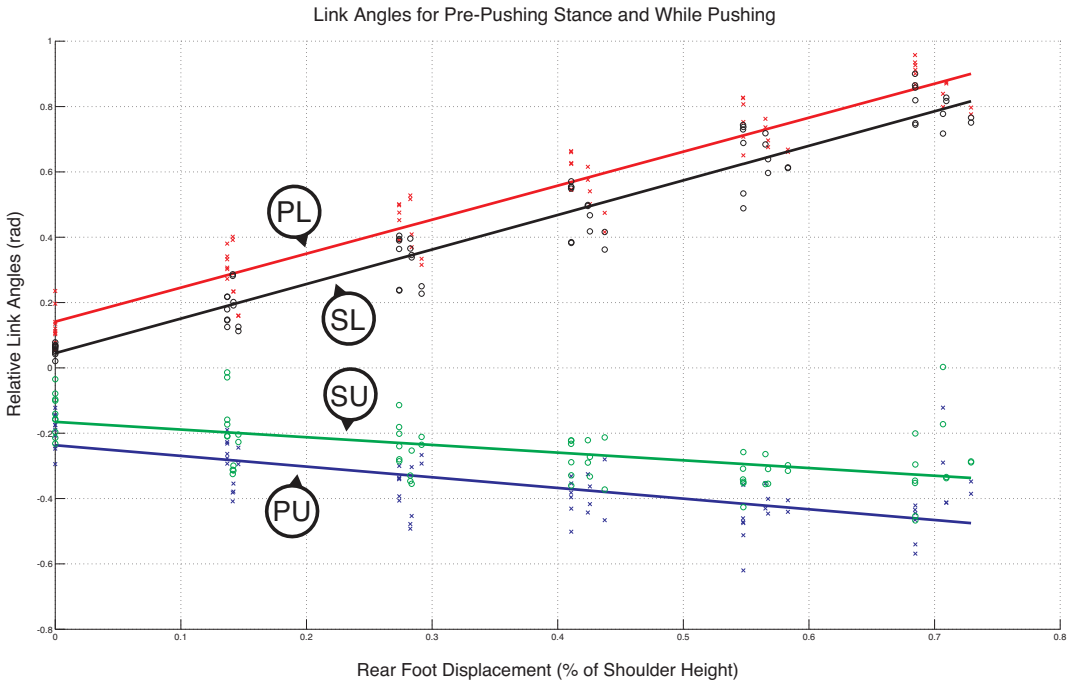

Figure 5.16: Relative angles (rad) in a **S**table pre-pushing stance and while **P**ushing for the **U**pper and **L**ower body links for all subjects and all foot displacements: *SU*, *SL*, *PU* and *PL*, respectively.

As seen in Figure 5.16, the angles of the upper and lower bodies are close in magnitude but opposite in direction when the foot displacement is under about 30% of the subject's shoulder height. This implies that the subject pushing is keeping their upper body near upright. This upper body orientation, along with the subject's moving of the hips forward, indicates that the subject is attempting to place their center of mass as far forward as possible given the constraints on allowable movement. Because the front foot remains in the same place throughout all tests, larger foot displacements show a more negative upper body angle but not negative enough to provide an upright posture. Instead, the subject is reaching for the pushing plane. Although reaching with the arms and body, a negative angle is maintained at the

waist to keep the shoulders high and the pushing force primarily horizontal. This observed forward movement of the ZMP prior to exerting a force at the hands allows for a greater force to be reached by providing a larger margin for backward ZMP movement.

Chapter 6: Humanoid Robot Experiment

6.1 HUBO+

HUBO+ is a mid-sized (130 cm) humanoid robot developed by Dr. Jun Ho Oh and graduate students at the Korean Advanced Institute of Technology (KAIST), in Daejeon, South Korea. The robot weighs in at 45kg. With 38 degrees of freedom (DOF, 6 in each arm and leg, 5 in each hand, 1 in waist, 3 in neck), the robot has been the platform for research in humanoid walking, running stability on uneven terrain. Stair climbing, object manipulation and ball throwing have also been demonstrated using this mechanically capable humanoid. HUBO+ is the newest iteration of KAIST humanoid robots (KHR-1,2,3,4) and is a upgraded of the KHR-4. Six of these models currently exist in the United States and act as a standardized research platform for collaboration between Drexel and other American universities.

6.2 Experiment

Using our humanoid robot, it was desired to experimentally show the increase in pushing force available when using a double inverted pendulum model over the single inverted pendulum model used in past pushing research (see Chapter 3).

Three stances were designed to explore the effect of a pre-pushing ZMP location on the applicable pushing force at the hands:

- **1. Single Inverted Pendulum:** aligned upper body and extended back leg at positive 20 degrees from vertical with a mass distribution of 80% on the front foot and 20% at the rear.
- **2. Double Inverted Pendulum, forwardmost ZMP:** with the same stance width and shoulder height of the single IVP test, a stance was found which places the ZMP as far forward as geometrically possible.
- **3. Double Inverted Pendulum, upright upper body:** with the same stance width and shoulder height of the single IVP test, a stance was found allowing the vertical orientation of the upper body.

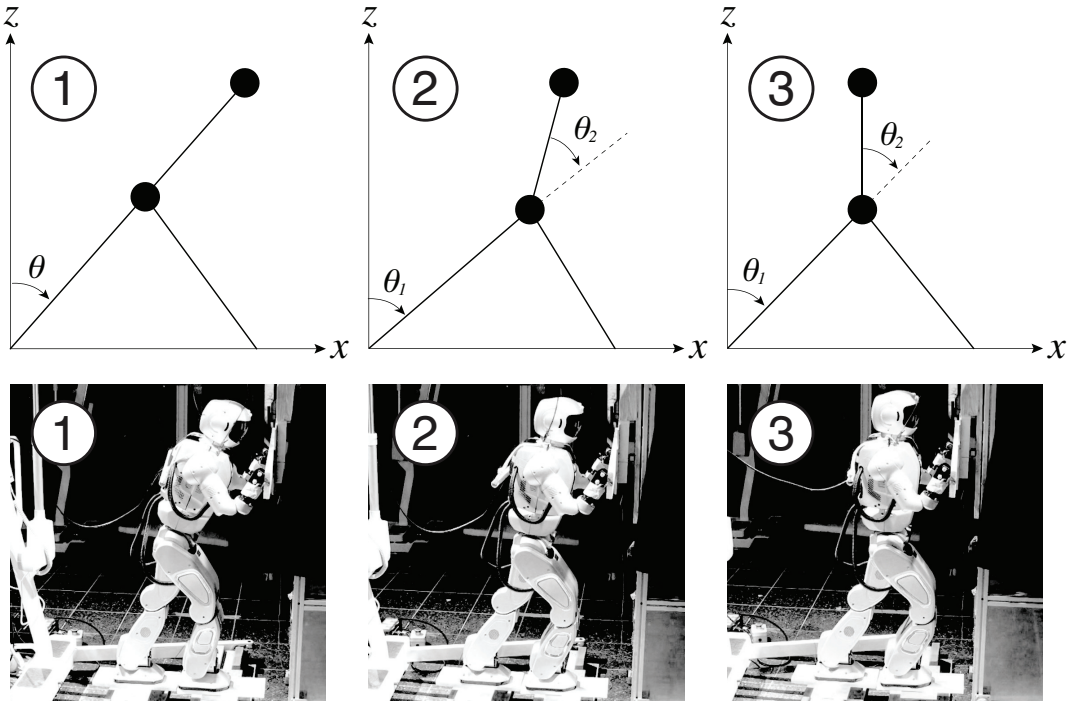

Figure 6.1: Humanoid robot, HUBO+, pushing in three different poses.

The stance length, held constant throughout, was determined using the double inverted pendulum model for our humanoid as defined in section 4.2. Using this model, the stance length was determined for the aligned upper body and extended back leg stance to produce a mass distribution of 80% on the front foot and 20% on the back foot prior to pushing. This procedure lead to a stance length of 30 cm between

the front and rear foot. The feet were aligned on the sagittal plane to eliminate the need to shift the ZMP on the sagittal axis to maintain stability.

For the two double inverted pendulum stances, the stance length and shoulder height were the same as in the single inverted pendulum stance. With these given constraints, two stances with different ZMP locations were realized. The first DIVP stance held the upper body upright (vertical). The second DIVP stance placed the ZMP as far forward as possible given the geometric constrains on the foot positions, the rear leg extension, and the shoulder height. The exploration of the joint configuration space given these constrains can be seen Figure 6.2.

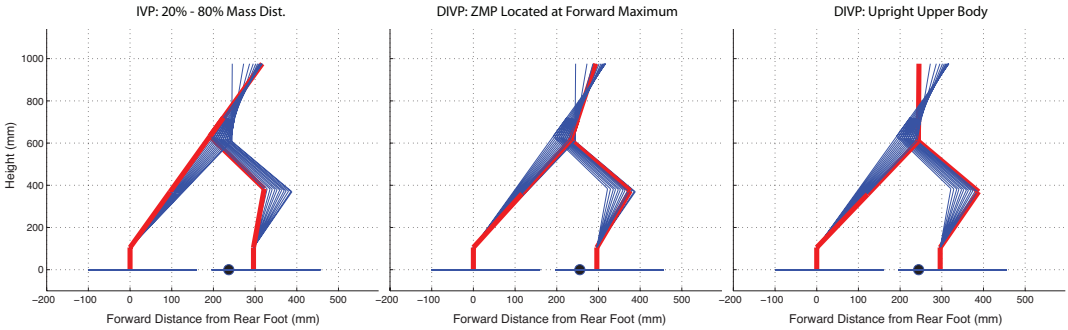

Figure 6.2: Three HUBO+ pushing poses with foot placement and shoulder height kept constant. The center stance shows the maximum forward location of the ZMP given these constraints.

As in the human tests, force plates were placed at the feet and the hands to determine the reaction forces during pushing. Two tests were conducted for each of the three stances to determine the effect of ZMP location on force exerted at the hands. For each test, the humanoid slowly extended the shoulder-level end effectors horizontally from a position of no contact to a point where the reaction force on the front foot was zero.

6.3 Results

As supported by human testing and mathematical simulation, the humanoid pose in which the ZMP location if furthest forward produced the highest pushing force at the hands. Furthermore, the experimental results for reaction force versus the ZMP location as the robot pushed matched the simulated results of the double inverted pendulum model much more closely than those of the single inverted pendulum model.

In comparing the simulation and experimental results for pushes originating in the three pre-pushing stances tested, the stance in which the ZMP is placed at in the forwardmost position yields the highest pushing force at the hands (Figure 6.3). The simulation data was obtained using a double inverted pendulum model of the humanoid with a 30 kg mass at the waist and a 17 kg mass at the chest. It can be seen that the simulation well represented the magnitude of forces exerted for a given ZMP location. Also gathered from these plots is the inconsistency in the aligned body and upright body simulation versus the experimental results. This can likely be attributed to error in the mass distribution used in the model along with inherent error in the simplification of a humanoid to a DIVP model.

The three pushing poses shown in Figure 6.1 can be separately compared to the single and double inverted pendulum simulations of the same pose (Figure 6.4). It is evident that the simulation using the double inverted pendulum model is more consistent with the experimental results than that of the single inverted pendulum model. The small disparity in slopes between the DIVP model and the experimental results can be attributed to error in the mass distribution used when modeling. With

tuning of these values, a model can be found that matches the experimental data more closely. In referencing the plots for each of the three tests, even more evident is the error associated in using a single inverted pendulum model to approximate the pushing capabilities of the humanoid.

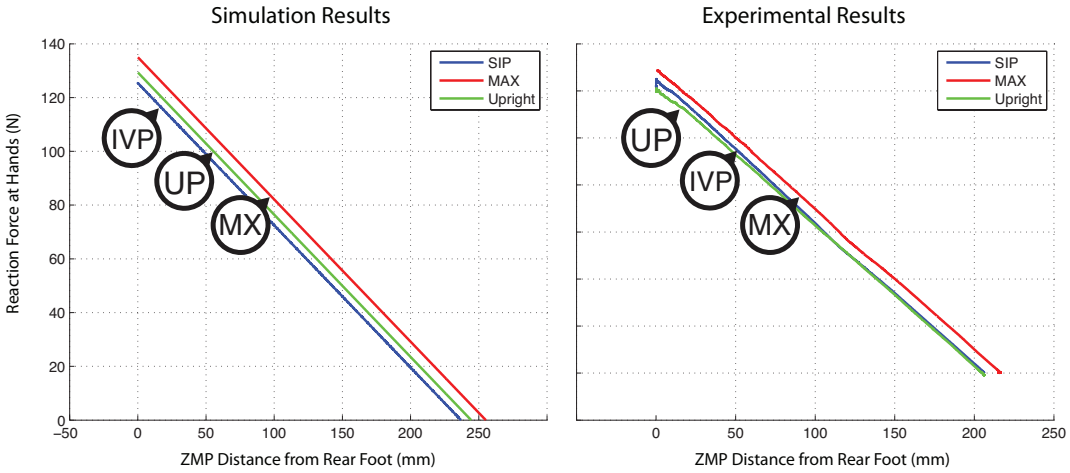

Figure 6.3: Reaction force versus ZMP location for a double inverted pendulum simulation of HUBO+ and the corresponding experimental results. IVP: Single inverted pendulum, UP: Upright upper body, MX: ZMP at maximum forward location.

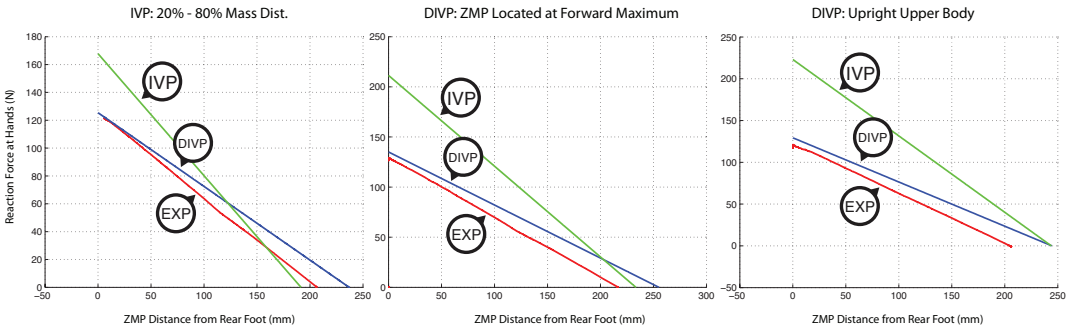

Figure 6.4: Comparison of the experimental data and simulation data of the DIVP and IVP models for each of the three poses tested. IVP: Single inverted pendulum, DIVP: Double inverted pendulum, EXP: Experimental results.

Chapter 7: Discussion

While the force and motion data of the subjects tested are analyzed with liberal estimation methods, trends supporting the advantage of waist articulation are easily observed. It was shown in Chapter 5 that, when allowed to rotate the upper body relative to the extended back leg, the CoM, and therefore the static ZMP, was positioned further forward than if the upper and lower bodies were kept aligned. This allowed the subject a larger ZMP margin while pushing and, therefore, the exertion of a larger range of forces and a larger maximum force overall (section 5.2.1). This forward position of the ZMP is limited by the flexibility of the ankle, knee, hip and waist, by the constraint on pushing level (shoulder height), and by the positions of the feet.

The analysis of human pushing also made evident the benefit of a foot kept up front during pushing. Primarily, the front foot allowed for a stable stance to be assumed prior to hand contact with the pushing plane. In this stance, most of the weight falls on the front foot. This disparity in mass distribution is especially significant when the ZMP is pushed forward. Without the front foot to take this weight, the pusher must rely on the pushing plane for support.

For a humanoid, stability is always a primary concern and this feet-apart stance serves to maintain stability before, during and after pushing. The ability to actively change the weight distribution between these two feet allows a range of forces to be

exerted without the changing of foot location. This ability is to be compared to a feet-together stance where both feet are displaced back from the pushing plane. For a large angle, it is necessary to rely on the object being pushed for stability. As soon as static friction is overcome by the applied force, the object will move and stability will be compromised. For both the safety and the facility to exert a range of forces, the feet apart stance is undeniably more useful than a feet-together stance when exploring for the force necessary to move an object of an unknown mass.

It is worth noting that, in a feet-apart stance, the ZMP can be stably shifted to either extent of the support polygon is reached. This means that the feet-apart stance can also be used to exert pulling forces. This is not possible without a front front placed ahead of the initial ZMP location as, while pulling, the ZMP will move forward until the support polygon limit. Further, the ability to stably lean forward in this stance allows for increased manipulability when pushing. As the object being pushed begins to move, instead of losing stability, the pusher can lean forward and continue pushing until the ZMP reaches the front limit of the support polygon.

The use of a feet-apart, double inverted pendulum humanoid model overcomes some of the limitations presented in previous humanoid pushing research. In the work of Harada et al. [20], the humanoid robot is modeled using a single inverted pendulum with a concentrated mass at the waist. With an upper body constrained to a vertical orientation, both feet are parallel and displaced back from the pushing plane. While this stance does bring the CoM lower and further forward than that of aligned upper and lower links, the model still does not take into account the ZMP location contribution of the separate links. Because of the structure of a humanoid,

a double inverted pendulum model brings us closer to an accurate mathematical representation of the robot's physical capabilities. A higher degree of freedom model allows for the leveraging of these capabilities when seeking some optimal solution.

Furthermore, the use of the feet together stance in the methods of Harada, Motoi [22] and other humanoid pushing researchers allows for only a well defined push to be safely performed. With the feet apart, much more freedom is allowed by a much larger stability region without the support of the object being pushed. In a feet-apart stance, the robot is stable without making contact and can therefore exert an overwhelming force to the object. If the object moves a great amount, there is no loss of the robot's object-independent stability. Using a feet-apart stance allows the robot to exert no force, a minor force or a maximum force all without changing its stance. This ability opens the doors to learning algorithms for optimized humanoid stance selection and pushing methods, or, more simply, just the ability to increases force until a necessary pushing force is determined.

In the research of Rancourt and Hogan [1], the idea of a single inverted pendulum model was considered more literally. The human body was modeled as a single link with a distributed mass. This model was used to explore the effects of different methods, including the lifting of one leg to raise the CoM, on the ranges of forces able to be produced in a certain stance. In their paper, both feet-together and feet apart stances were considered. While Rancourt and Hogan did conclude that a feet-apart stance provided the ability to exert a much larger range of forces for a given body angle, the idea was never extended to a more complex model. Using a double inverted pendulum model for the humanoid has proven to extend this range of forces

available by providing another method of moving the CoM, and therefore the ZMP, forward prior to pushing.

The effect of locating the ZMP further forward by means of waist joint freedom has been observed in human pushing experiments and confirmed through mathematical simulation and humanoid robot testing. Future work includes further exploration of constraint flexibility, especially concerning the shoulder height, for finding the extreme anterior limit for ZMP placement. Further, the online control of ZMP location should allow the humanoid to effectively counteract a portion of its pushing force by moving its center of mass forward, even past its support polygon, while pushing, allowing a greater maximum force overall. These methods of ZMP placement and location control are relevant in the exertion of pushing and pulling forces, as well as for stance assumption in preparation of lifting an object, turning a valve, using some tools or, generally, any exertion or endurance of unknown external force.

Chapter 8: Conclusion

Through human motion and reaction force analysis, it was realized that a larger range of forces could be exerted in a feet-apart stance (one foot displaced back from the pushing plane) than in a feet-together stance (both feet parallel and displaced back). Furthermore, this range of forces is increased if the subject is allowed movement of the waist, enabling them to shift the hips and upper body, and therefore the ZMP location, forward prior to pushing. This observation lead to the consideration of a double inverted pendulum model for humanoid robot pushing over the commonly used single inverted pendulum model. Using this two-link, two-mass model, a humanoid robot was able to exert more force at the hands with no compromise of stability. The forces to be exerted by the humanoid in the stances tested were predicted using the single and double inverted pendulum models of the robot. While the DIVP predicted both the magnitude and slope of ZMP location versus exerted force with only minor error, the IVP model was extremely inaccurate. Using a double inverted pendulum model a log with a feet apart stance allows for predicable, adjustable and stable force exertion.

Bibliography

[1] Denis Rancourt and Neville Hogan. Dynamics of pushing. *Journal of motor behavior*, 33(4):351–62, 2001.

[2] M. Vukobratovic and J. Stepanenko. On the stability of anthropomorphic systems. *Mathematical Biosciences*, 15(12):1 – 37, 1972.

[3] S. Sugano and I. Kato. Wabot-2: Autonomous robot with dexterous finger-arm–finger-arm coordination control in keyboard performance. In *Robotics and Automation. Proceedings. 1987 IEEE International Conference on*, volume 4, pages 90 – 97, mar 1987.

[4] K. Hirai. Current and future perspective of honda humamoid robot. In *Intelligent Robots and Systems, 1997. IROS '97., Proceedings of the 1997 IEEE/RSJ International Conference on*, volume 2, pages 500 –508 vol.2, sep 1997.

[5] K Hirai, M Hirose, Y Haikawa, and T Takenaka. The development of honda humanoid robot. *IEEE International Conference on Robotics and Automation Proceedings*, 2:1321–1326, 1998.

[6] Y. Sakagami, R. Watanabe, C. Aoyama, S. Matsunaga, N. Higaki, and K. Fujimura. The intelligent asimo: system overview and integration. In *Intelligent Robots and Systems, 2002. IEEE/RSJ International Conference on*, volume 3, pages 2478 – 2483 vol.3, 2002.

[7] J. Chestnutt, P. Michel, J. Kuffner, and T. Kanade. Locomotion among dynamic obstacles for the honda asimo. In *Intelligent Robots and Systems, 2007. IROS 2007. IEEE/RSJ International Conference on*, pages 2572 –2573, 29 2007-nov. 2 2007.

[8] Ltd. Honda Motor Co. Honda unveils all-new asimo with significant advancements. Press release information, 2011.

[9] J. Yamaguchi, E. Soga, S. Inoue, and A. Takanishi. Development of a bipedal humanoid robot-control method of whole body cooperative dynamic biped walking. In *Robotics and Automation, 1999. Proceedings. 1999 IEEE International Conference on*, volume 1, pages 368 –374 vol.1, 1999.

[10] K. Kaneko, F. Kanehiro, S. Kajita, H. Hirukawa, T. Kawasaki, M. Hirata, K. Akachi, and T. Isozumi. Humanoid robot hrp-2. In *Robotics and Automation, 2004. Proceedings. ICRA '04. 2004 IEEE International Conference on*, volume 2, pages 1083 – 1090 Vol.2, 26-may 1, 2004.

[11] K. Kaneko, F. Kanehiro, M. Morisawa, K. Akachi, G. Miyamori, A. Hayashi, and N. Kanehira. Humanoid robot hrp-4 - humanoid robotics platform with lightweight and slim body. In *Intelligent Robots and Systems (IROS), 2011 IEEE/RSJ International Conference on*, pages 4400 –4407, sept. 2011.

[12] M. Gienger, K. Loffler, and F. Pfeiffer. Towards the design of a biped jogging robot. In *Robotics and Automation, 2001. Proceedings 2001 ICRA. IEEE International Conference on*, volume 4, pages 4140 – 4145 vol.4, 2001.

[13] Ill-Woo Park, Jung-Yup Kim, Jungho Lee, and Jun-Ho Oh. Mechanical design of humanoid robot platform khr-3 (kaist humanoid robot 3: Hubo). In *Humanoid Robots, 2005 5th IEEE-RAS International Conference on*, pages 321 –326, dec. 2005.

[14] A. Goswami. Foot rotation indicator (fri) point: a new gait planning tool to evaluate postural stability of biped robots. In *Robotics and Automation, 1999. Proceedings. 1999 IEEE International Conference on*, volume 1, pages 47 –52 vol.1, 1999.

[15] S. Kajita, F. Kanehiro, K. Kaneko, K. Fujiwara, K. Harada, K. Yokoi, and H. Hirukawa. Biped walking pattern generation by using preview control of zero-moment point. In *Robotics and Automation, 2003. Proceedings. ICRA '03. IEEE International Conference on*, volume 2, pages 1620 – 1626 vol.2, sept. 2003.

[16] Ill-Woo Park, Jung-Yup Kim, and Jun-Ho Oh. Online biped walking pattern generation for humanoid robot khr-3(kaist humanoid robot - 3: Hubo). In *Humanoid Robots, 2006 6th IEEE-RAS International Conference on*, pages 398 –403, dec. 2006.

[17] S. Kajita, T. Nagasaki, K. Kaneko, and H. Hirukawa. Zmp-based biped running control. *Robotics Automation Magazine, IEEE*, 14(2):63 –72, june 2007.

[18] Hyeonsik Shin and Jong Hyeon Park. Zmp-based biped running pattern generation with contact transition of foot. In *Advanced Intelligent Mechatronics, 2008. AIM 2008. IEEE/ASME International Conference on*, pages 916 –921, july 2008.

[19] B. Ugurlu and A. Kawamura. Real-time running and jumping pattern generation for bipedal robots based on zmp and euler's equations. In *Intelligent Robots and Systems, 2009. IROS 2009. IEEE/RSJ International Conference on*, pages 1100 –1105, oct. 2009.

[20] K. Harada, S. Kajita, K. Kaneko, and H. Hirukawa. Pushing manipulation by humanoid considering two-kinds of zmps. In *Robotics and Automation, 2003. Proceedings. ICRA '03. IEEE International Conference on*, volume 2, pages 1627 – 1632 vol.2, sept. 2003.

[21] Kensuke Harada, Shuuji Kajita, Fumio Kanehiro, Kiyoshi Fujiwara, Kenji Kaneko, Kazuhito Yokoi, and Hirohisa Hirukawa. Real-time planning of

humanoid robot's gait for force-controlled manipulation. *Mechatronics, IEEE/ASME Transactions on*, 12(1):53 –62, feb. 2007.

[22] N. Motoi, M. Ikebe, and K. Ohnishi. Real-time gait planning for pushing motion of humanoid robot. *Industrial Informatics, IEEE Transactions on*, 3(2):154 –163, may 2007.

[23] M. Stilman, K. Nishiwaki, and S. Kagami. Humanoid teleoperation for whole body manipulation. In *Robotics and Automation, 2008. ICRA 2008. IEEE International Conference on*, pages 3175 –3180, may 2008.

[24] M. Stilman, K. Nishiwaki, and S. Kagami. Learning object models for whole body manipulation. In *Humanoid Robots, 2007 7th IEEE-RAS International Conference on*, pages 174 –179, 29 2007-dec. 1 2007.

[25] Yoonkwon Hwang, A. Konno, and M. Uchiyama. Whole body cooperative tasks and static stability evaluations for a humanoid robot. In *Intelligent Robots and Systems, 2003. (IROS 2003). Proceedings. 2003 IEEE/RSJ International Conference on*, volume 2, pages 1901 – 1906 vol.2, oct. 2003.

[26] S. Kajita and K. Tani. Study of dynamic biped locomotion on rugged terrain-derivation and application of the linear inverted pendulum mode. In *Robotics and Automation, 1991. Proceedings., 1991 IEEE International Conference on*, pages 1405 –1411 vol.2, apr 1991.

[27] W. T. Dempster. Analysis of two-handed pulls using free body diagrams. *Journal of Applied Physiology 1958 Nov ;13 (3):469-80*, 13:469–480, 1958.

[28] R. O. Andres D. B. Chaffin and A. Garg. Volitional postures during maximal push/pull exertions in the sagittal plane. *Human Factors: The Journal of the Human Factors and Ergonomics*, 25:541–550, 1983.

[29] M. M. Ayoub and J. W. McDaniel. Effects of operator stance on pushing and pulling tasks. *AIIE Transactions*, 6:185–195, 1974.

[30] B. J. Daams. Static force exertion in postures with different degrees of freedom. *Ergonomics*, 36:397–406, 1993.

[31] S. Kajita and B. Espiau. Legged robots. In *Springer Handbook of Robotics*, pages 361–389, 2008.

[32] K. H. E. Kroemer, K. E. Kroemer-Elbert, and H. B. Kroemer. *Ergonomics : how to design for ease and efficiency / K.H.E. Kroemer, H.B. Kroemer, K.E. Kroemer-Elbert.* Prentice Hall, Englewood Cliffs, NJ :, 1994.

[33] Andersson Gunnar B. J. Chaffin, D. B. and Bernard J. Martin. *Occupational Biomechanics.* Wiley, Toronto, Ontario :, 1991.

Appendix A: List of Abbreviations

CoM: Center of Mass

CoP: Center of Pressure

DIVP: Double inverted pendulum

DOF: Degrees of freedom

DSP: Double support phase

GUI: Graphical user interface

IVP: Inverted pendulum

SSP: Single support phase

ZMP: Zero-moment point